ACS Energy LETTERS

Cite This: ACS Energy Lett. 2019, 4, 1134−1149

http://pubs.acs.org/journal/aelccp

PERSPECTIVE

# Boosting Efficiency in Polycrystalline Metal Halide Perovskite Light-Emitting Diodes

Min-Ho Park,[†,‡,#] Joo Sung Kim,[†,#] Jung-Min Heo,[†,#] Soyeong Ahn,[∥] Su-Hun Jeong,[†] and Tae-Woo Lee*[,†,‡,§]

[†]Department of Materials Science and Engineering, BK21 PLUS SNU Materials Division for Educating Creative Global Leaders Seoul National University, 1 Gwanak-ro, Gwanak-gu, Seoul 08826, Republic of Korea

[‡]Research Institute of Advanced Materials, Seoul National University, 1 Gwanak-ro, Gwanak-gu, Seoul 08826, Republic of Korea

[§]Institute of Engineering Research, Nano System Institute (NSI), Seoul National University, 1 Gwanak-ro, Gwanak-gu, Seoul 08826, Republic of Korea

[∥]Department of Materials Science and Engineering, Pohang University of Science and Technology (POSTECH), 77 Cheongam-Ro, 10 Nam-Gu, Pohang, Gyeongbuk 37673, Republic of Korea

**ABSTRACT:** **Metal halide perovskites (MHPs) have outstanding photophysical properties and are therefore being evaluated as next-generation light emitters. Within just a few years, the efficiencies of polycrystalline perovskite light-emitting diodes (PeLEDs) have been drastically improved and are catching up with those of conventional organic LEDs. The electroluminescence efficiency of polycrystalline PeLEDs has been limited by shortcomings such as limited outcoupling efficiency, charge imbalance in MHP emitting layers, difficulty controlling surface morphology, small exciton binding energy at room temperature, and nonradiative recombination at defect sites. In this Perspective, we focus on promising strategies such as optical engineering, charge balance control, morphological and nanograin engineering, and chemical modification to overcome these shortcomings and suggest future directions for research to further improve the efficiencies of polycrystalline PeLEDs.**

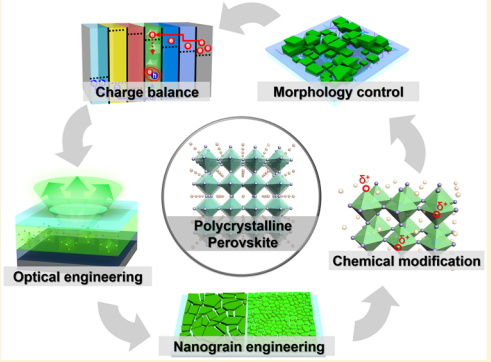


Metal halide perovskites (MHPs) are promising semiconducting materials for next-generation optoelectronic devices.[1−4] Through the development history of organic light-emitting diodes (OLEDs) for about the last 30 years, OLED displays have evolved into thin, lightweight, and curved forms with high resolution and superior electroluminescence (EL) efficiencies for low energy consumption. However, the high material cost and low color purity of organic emitting materials do not meet the need for a low-cost product with a vivid, natural color display. Therefore, to make the leap into the development of next-generation luminescent materials that meet those needs, MHPs have quickly attracted the attention of researchers studying LEDs because MHPs have excellent photophysical properties, including high color purity with narrow full width at half-maximum (FWHM) of photoluminescence (PL), excellent electrical properties, simple solution processability at low temperature, and easy synthesis routes.[5−7]

Three-dimensional (3D) polycrystalline MHPs have $ABX_3$ crystal structure, where A is an organic or inorganic cation that functions as a structural template, B a metal cation, and X a halide anion.[8−10] Each B is surrounded by six X atoms, and each A is positioned in the center of $BX_6$ octahedral frameworks. To be structurally stable, polycrystalline MHPs should have the tolerance factor $t = (r_A + r_X)/[\sqrt{2}\ (r_B + r_X)]$, where $r$ is the ionic radius, in the range $0.8 \leq t \leq 1.0$, and octahedral factor ($\mu = r_B/r_X$) in the range $0.44 \leq \mu \leq 0.9$, respectively.[9,11,12] The crystal structure of 3D cesium-based lead halides ($CsPbX_3$; X = Cl, Br, I) was first investigated by Møller in 1958,[13] and 3D methylammonium (MA)-based MHPs ($CH_3NH_3BX_3$; $CH_3NH_3$ = MA; B = Pb, Sn; X = Br, I) were first synthesized by Weber in 1978.[14,15] Since then, the optical, photophysical, structural, and dielectric properties of MHPs have been tested at various temperature ranges.[16−20] Some early works reported MHP LEDs (PeLEDs);[21−26] such PeLEDs worked at low temperature (<110 K) in the 1990s, but had relatively wide FWHM of 100 nm at room temperature, as a result of emission from organic fluorescent ligands instead of the Pb−X octahedron lattice in 1999.[26] These reports did not receive much attention because the low-

Received: March 8, 2019
Accepted: April 15, 2019
Published: April 15, 2019

Downloaded via SEOUL NATL UNIV on December 22, 2020 at 06:49:25 (UTC).
See https://pubs.acs.org/sharingguidelines for options on how to legitimately share published articles.


© 2019 American Chemical Society

DOI: 10.1021/acsenergylett.9b00518
ACS Energy Lett. 2019, 4, 1134−1149

temperature processing or wide-band emission are not appropriate for next-generation emitting devices.[21−26] Thermal exciton quenching (i.e., thermal ionization of excitons) may be the main cause of the low EL efficiency of 3D polycrystalline PeLEDs at room temperature;[24] if this is correct, then EL efficiency of PeLEDs could be increased by achieving a high radiative recombination rate at room temperature. This early work on PeLEDs showed a low possibility of MHPs as emitters at room temperature and did not investigate engineering methods such as morphology and grain size controls, interface modification, or use of additives to overcome the EL efficiency limitations.

3D polycrystalline MHPs were first chosen for use in light emitters for PeLEDs because of the advantages of simple synthesis, easy film fabrication, and effective charge-transporting properties.

3D polycrystalline MHPs were first chosen for use in light emitters for PeLEDs because of the advantages of simple synthesis, easy film fabrication, and effective charge-transporting properties.[1,2,7,27] In 2014, the first PeLEDs that had been developed at room temperature using 3D polycrystalline MHP emitters with $MAPbI_{3-x}Cl_x$ and $MAPbBr_3$ were produced by adopting simple planar structures, which had solution-processed MHP emitting layers (EMLs) between charge-transporting organic layers with electrodes.[2,28] The EL efficiencies of the early-stage PeLEDs in 2014 [infrared (IR) radiance of 13.2 W/(sr·m$^2$) and external quantum efficiency (EQE) = 0.76% for $MAPbI_{3-x}Cl_x$; luminance $L$ = 417 cd/m$^2$ and EQE of 0.125% for $MAPbBr_3$ perovskite emitters][2,28] were inferior to those of conventional OLEDs, but those solution-processed PeLEDs clearly proved the possibility of room-temperature processed next-generation LEDs with a high color purity of a narrow FWHM ≈ 20 nm. Therefore, this pioneering work triggered research in PeLEDs.[2,28] Since then, EQEs of PeLEDs have been dramatically improved to the EQE level of OLEDs; therefore, PeLEDs have been proven to be promising next-generation LEDs.[1,4,29−32] This rapid increase of EQE in visible-emitting PeLEDs is much faster than that of the conventional OLEDs (Figure 1A). This increase may be a result of high purity of semiconducting materials that can be achieved by improved synthesis methods and of the highly developed solution-processing and vacuum-processing techniques for device fabrication which have been established through the development of OLEDs over the last few decades.

Recently achieved EQEs of ∼20% clearly prove the possibility of 3D MHPs as next-generation light emitters.[33−36] An island/lid-stacked structure (termed quasi-core/shell) of polycrystalline $CsPbBr_3$ capped with MABr additive yielded EQE = 17% [current efficiency (CE) = 65 cd/A] in green polycrystalline PeLED.[33] This structure allowed high photoluminescence quantum yield (PLQY). The EQE was maximized to 20.31%, assuming a Lambertian distribution ($CE_{max}$ = 78 cd/A, $CE_{min}$ ≈ 42.5 cd/A, average CE ≈ 56.75 cd/A with relative standard deviation ∼ 17.9%) by inserting a thin insulating poly(methyl methacrylate) (PMMA) layer to improve charge balance.[33] Increase in light extraction efficiency in polycrystalline PeLEDs based on submicrometer-scale $FAPbI_3$ (FA = formamidinium) yielded maximum EQE = 20.7% (minimum EQE ≈ 17.75%, average EQE ≈ 19.2% with relative standard deviation of 4%) with invisible IR emission.[34] The increase in light extraction from $FAPbI_3$ was achieved using an insulating layer of 5-aminovaleric acid (5AVA) to reduce leakage current through the uncovered emitter region and to passivate surface defects. Those rapid developments of PeLEDs have confirmed their possibility of utility as next-generation emitters.

However, the high relative standard deviation of reported EQEs are still problematic; therefore, a reliable method to produce high-efficiency PeLEDs with narrow EQE distribution should be developed. In this Perspective, we present promising strategies for efficient 3D polycrystalline films and cover the prospective ways to effectively improve their EL efficiency of polycrystalline PeLEDs (Figure 1B).

*Optical Engineering and Charge Balance Control.* The intrinsic properties of MHPs such as long electron−hole diffusion length, small exciton binding energy at room temperature, and high extinction coefficient (i.e., strong light absorption) are not favorable for LED applications that in principle need a high radiative recombination rate with low defect density, effective exciton confinement, low optical loss, and charge balance in PeLEDs. To satisfy those requirements in 3D MHP films, optical properties and charge balance should be modified during deposition of the MHP film and fabrication of the devices.

Multilayer PeLEDs are composed of MHP EMLs, organic charge transport layers, and electrodes. Optical energy loss in planar LEDs is a result of the surface plasmon, waveguide mode, and substrate mode. Especially, the refractive index $n$ is generally higher in solution-processed MHP films ($n$ ≈ 2.2−2.6) than in organic films ($n$ ≈ 1.4−2.0), so $n$ can differ greatly across the interface between them. As a result, the waveguide mode of the total reflection of the emitting light at the interface of MHP EMLs can be a major optical energy loss in PeLEDs.[37,38] Therefore, modifying the optical properties is a simple but very effective approach to improve the light outcoupling of PeLEDs. Optical simulation to estimate theoretical EQE values of PeLEDs with assumptions of ideal charge balance, PLQY, and film conditions (i.e., without considering defects and surface morphology condition) showed that 3D polycrystalline $MAPbI_3$ PeLEDs can have $EQE_{max}$ (25.7%) that is relatively higher than that (19.6%) in quasi-2D $NFPI_7$ (the mixture of 1-naphthylmethylamine iodide, FA iodide, and Pb iodide) PeLEDs.[39] The simulation result suggested that the light interference effect can be induced by the high $n$ of 3D MHP films; therefore, the outcoupling effect can be improved by sensitively controlling the thickness of 3D MHP EMLs (Figure 2A,B).[39] The outcoupling effect in PeLEDs depends on the MHP EML thickness by designing a thin MHP layer (35−40 nm); the waveguide optical loss is significantly minimized to effectively improve light outcoupling and EQEs from 4.8% (160 nm thickness) to 14.3% (35 nm thickness) of the $MAPbI_3$ PeLEDs (Figure 2C).[38] Reducing the $n$ of MHP films can also be effective to minimize waveguide mode optical loss in PeLEDs (Figure 2D). The $n$ is influenced by the density of the material or porosity; the Lorentz−Lorenz relationship states that low density of MHP films can lead to a low $n$.[40,41] The light emitted from the MHP EMLs passes through complex media, including grains and grain boundary regions that form during the crystallization process. The density of the crystallized MHP



DOI: 10.1021/acsenergylett.9b00518
ACS Energy Lett. 2019, 4, 1134−1149

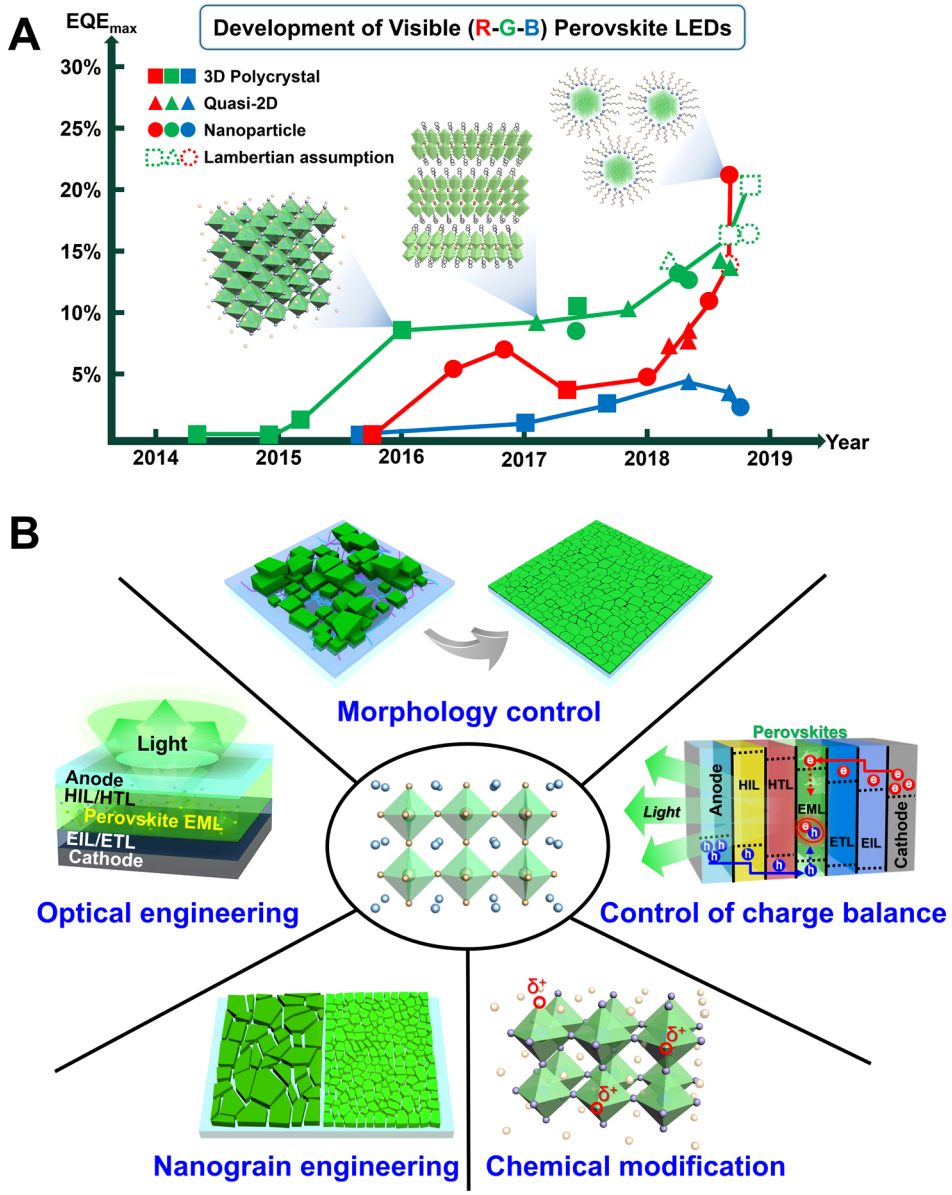


**Figure 1. (A) EQE developments depending on the dimension of metal halide perovskites. (B) Promising strategies for highly efficient polycrystalline PeLEDs.**

films can be affected by the deposition method and crystallinity; therefore, the $n$ of MHP films can be changed. In single-crystalline MHP, $n$ = 2.5; in solution-processed MHP, $n$ = 2.2; and in vacuum-processed MHP films, $n$ = 1.8 (Figure 2E).[42] The decrease in $n$ means that the polycrystalline media had lower $n$ than the single-crystalline MHP because the solution-processed MHP film can have relatively lower density and suggests that the lowest $n$ of vacuum-processed MHP film may originate from a lower density, which can be caused by a low crystallinity. Optical simulation indicated that as $n$ decreased from 2.5 to 1.6 (i.e., decrease by 36%), the outcoupling efficiencies improved from 7% to 25% (i.e., increase by 350%).[42] Therefore, controlling optical properties (i.e., the $n$ and thickness) of MHP films and design of device architecture are highly effective approaches to achieve optimal EQEs in PeLEDs when ideal MHP films are deposited.

EL efficiency in LEDs is significantly determined by the charge balance, recombination rate of electron–hole pairs, and PLQY of the emitting film in devices. Compared to 3D

EL efficiency in LEDs is significantly determined by the charge balance, recombination rate of electron–hole pairs, and PLQY of the emitting film in devices.

polycrystalline MHPs, the low-dimensional [two-dimensional (2D) or zero-dimensional (0D)] MHPs have higher exciton binding energies and effective exciton confinements due to quantum confinement effects by large insulating organic cations or organic ligands.[3,43−45] In 2D MHPs, a few $PbX_6$ (X = Cl, Br, I) layers are sandwiched by adding bulky organic cations such as phenylethylammonium (PEA) or butylammonium (BA) to achieve a multiquantum well structure that yields large exciton binding energy and strong exciton confinement.[46] In 0D MHPs, $PbX_6$ octahedra that are isolated by insulating ligands effectively confine excitons; this results in



DOI: 10.1021/acsenergylett.9b00518
ACS Energy Lett. 2019, 4, 1134−1149

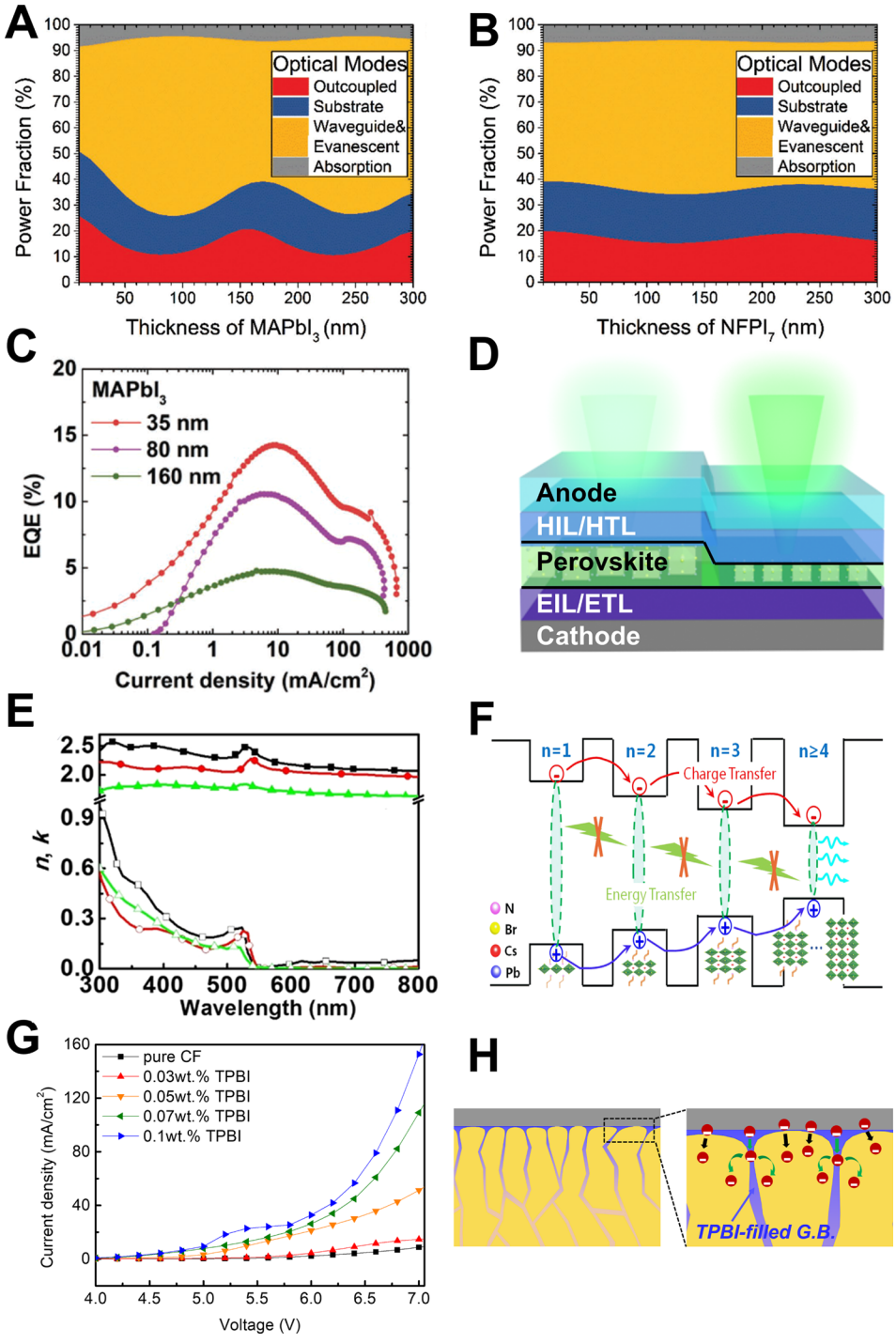


**Figure 2. Optical power distribution of (A) 3D $MAPbI_3$ ($n$ = 2.6) and (B) quasi-2D $NFPI_7$ ($n$ = 2.0) PeLEDs depending on the MHP EML thickness. (Adapted with permission from ref 39. Copyright 2018 Wiley Online Library.) (C) External quantum efficiencies of PeLEDs depending on the $MAPbI_3$ thickness. (Adapted with permission from ref 38. Copyright 2018 Wiley Online Library.) (D) Schematic illustration of optical outcoupling in polycrystalline PeLEDs depending on the EML thickness. (E) Optical constants (filled symbol, $n$; open symbol, $k$) of single crystal (black), solution-processed thin-film (red), and vacuum-processed thin-film (green) from ellipsometry measurements. (Adapted from ref 42. Copyright 2017 American Chemical Society.) (F) Schematic images of energy and charge carrier cascade in multiquantum wells of quasi-2D MHPs. (Adapted with permission from ref 35. Copyright 2018 Elsevier Ltd.) (G) Electron current density versus voltage measurement of $MAPbBr_3$-based electron-dominant devices depending on the TPBI additive concentration of A-NCP. (Adapted with permission from ref 30. Copyright 2017 Elsevier Ltd.) (H) Schematic illustration of improved electron injection efficiency at the MHP interface. (Adapted with permission from ref 30. Copyright 2017 Elsevier Ltd.).**

high exciton binding energy.[47,48] Furthermore, $CsPbX_3$ (X = halides) quantum dots (QDs) have achieved PLQY > 90%.[49] The low dimensionalities of 2D and 0D MHPs are theoretically beneficial to achieving high external PLQY of the films, which can lead to high EL efficiency. However, the external PLQY of the MHP films can be decreased by photon recycling and low outcoupling efficiency that arise from the high $n$ of MHPs.[37,50] Therefore, passivation of surface defects



DOI: 10.1021/acsenergylett.9b00518
ACS Energy Lett. 2019, 4, 1134−1149

in 3D polycrystalline $MAPbI_3$ film has given a high internal PLQY = 91.9% at the photon flux of 60 mW/cm$^2$ at 532 nm, although an external PLQY showed 37%.[37,50] This high internal PLQY of 3D MHPs suggests that 3D polycrystalline MHP films possibly have a high radiative recombination rate, but high external PLQY may be degraded by bulk and surface defects and by high $n$. Therefore, an ideal EQE up to 25−30% in 3D polycrystalline PeLEDs can be achieved when the low external PLQY is overcome by defect passivation and effective light outcoupling.

Although the grain boundary has been reported as a charge-transporting barrier, charge separator, and charge trapping site in 3D MHPs,[27,51] the charge-transporting property is more beneficial in 3D MHPs than in 2D and 0D PeLEDs that have bulky organic cations or insulating ligands.[52] Furthermore, the contribution of the charge transfer is more important than the energy transfer for the EL efficiency of quasi-2D $PA_2(CsPbBr_3)_{y-1}PbBr_4$ PeLEDs (PA = propylammonium; $y$ = number of $PbBr_6$ layers between bulky organic layer) accompanied by efficient energy confinement during electrical device operation (Figure 2F).[35] Especially, the charge balance and confinement depending on charge carrier cascades from high to low bandgap states (i.e., MHP units with large $y$) in quasi-2D MHP films are not efficient because of the energy level differences between multiquantum well MHP units and the imbalanced electron and hole cascade;[35] charges can accumulate and device efficiency can decrease significantly at high driving voltages. Therefore, the charge-transporting property is an important parameter in the luminescent properties of PeLEDs; the electrical transport property can be better when 3D MHPs are used than when low-dimensional MHPs are used, and the efficiency of the PeLEDs can be effectively improved when the defective grain boundary region becomes benign.

To further improve the charge balance in PeLEDs, the charge injection efficiency at the interface of MHP EMLs should be considered. The surface of crystallized MHP EMLs has a high density of grain boundary regions that significantly suppress the charge injection and transport because of poor interfacial characteristics such as contact barriers, charge scattering, and defects including vacancies and interstitials.[27,53,54] The charge carrier mobility $\mu$ in MHPs is significantly influenced by the crystallinity and grain size of MHP films, and these characteristics can be strongly affected by the deposition methods.[55] As grain size decreases, grain boundary region increases; therefore, $\mu$ is significantly lower in polycrystalline $MAPbBr_3$ [$\mu$ = 0.047 cm$^2$/(V·s)] than in a single $MAPbBr_3$ crystal [$\mu$ = 38 cm$^2$/(V·s)].[27,30,56,57] $\mu$ can be increased by passivating the defective grain boundary regions by filling it with organic semiconducting molecules to suppress the charge scattering and improve interfacial characteristics; the result is an increase in charge injection efficiency and charge balance in the devices. In the standard-structured $MAPbBr_3$ PeLEDs, the electron injection efficiency can be improved by filling the grain boundary region near the $MAPbBr_3$ surface with a semiconducting organic additive such as 2,2′,2″-(1,3,5-benzinetriyl)-tris(1-phenyl-1-H-benzimidazole) (TPBI); this process increases the electron current density levels as TPBI additive concentration increases (Figure 2G,H).[30] The improved electron injection induced effective charge balance and thereby resulted in a gradual increase in EQEs from 2.56% to 8.79%. Moreover, both the hole and electron injection efficiencies for the charge balance can be simultaneously improved by a coadditive system of hole-transporting additive and an electron-transporting additive. The hole- and electron-transporting properties can be investigated by measuring the current density−voltage characteristics of unipolar charge-dominant devices.[30,58] The hole (or electron) current density can be increased when the hole-transporting (or electron-transporting) additive is added into MHP precursor solutions. An optimized 1:2 weight ratio of poly(9-vinylcarbazole) (PVK) as a hole-transporting additive and TPBI as electron-transporting additive improved charge balance in $MAPbBr_3$ PeLEDs and greatly increased the CEs from 1.4 cd/A to 9.45 cd/A.[58] Therefore, methods to optimize the devices should simultaneously include adding organic transporting materials into MHPs and applying optical engineering for effective light outcoupling by reducing $n$ and controlling electron−hole balance by composition engineering.

*Morphological Engineering*. Poor surface morphology and coverage cause nonradiative recombination loss, which is one of the critical problems that degrade the luminescent efficiency in planar PeLEDs, especially when the organic or MHP layers are deposited using a solution process.[59−62] The interfacial properties between layers of planar-structured devices are closely related to current leakage and device lifetime. Furthermore, 3D MHPs generally form micrometer-scale, island-like microscale cubic crystals with poor surface coverage after the normal spin-coating process because MHP precursors have poor wettability on the underlying organic layer and crystallize rapidly.[63] The discontinuous crystal domains and poor surface coverage are accompanied by pinholes, which can cause leakage current in the devices.[1,28] The direct contacts between charge transport layers due to pinholes between large cuboid MHP crystals can allow charges to pass through the devices without injecting charges into MHP EMLs; the charge transport can be concentrated in a local contact region and thereby significantly degrade the device efficiency of PeLEDs.[64−66] Therefore, strategies of morphological engineering to improve surface morphology for efficient PeLEDs have been reported.[67−71] The most representative method is the antisolvent-induced crystallization process, which can induce rapid and uniform crystallization of MHP crystals to achieve a pinhole-free and uniform morphology.[72−75] The smooth surface coverage without leakage current by discontinuous microcuboids can generally achieve improved device performance with high reproducibility in applications of both solar cells and LEDs.

> Poor surface morphology and coverage cause nonradiative recombination loss, which is one of the critical problems that degrade the luminescent efficiency in planar PeLEDs.

Simple control of the molar ratio between the MHP precursors such as MABr and $PbBr_2$ (i.e., stoichiometry engineering) can yield good surface morphology with high reproducibility and low nonradiative recombination loss by enabling sufficient reaction between excess MABr and $PbBr_2$.[65] The resulting PeLEDs have low current leakage; this is ascribed to the improved surface morphology and yielded PeLEDs that had improved $L_{max}$ = 6124 cd/m$^2$ and $CE_{max}$ =



DOI: 10.1021/acsenergylett.9b00518
ACS Energy Lett. 2019, 4, 1134−1149

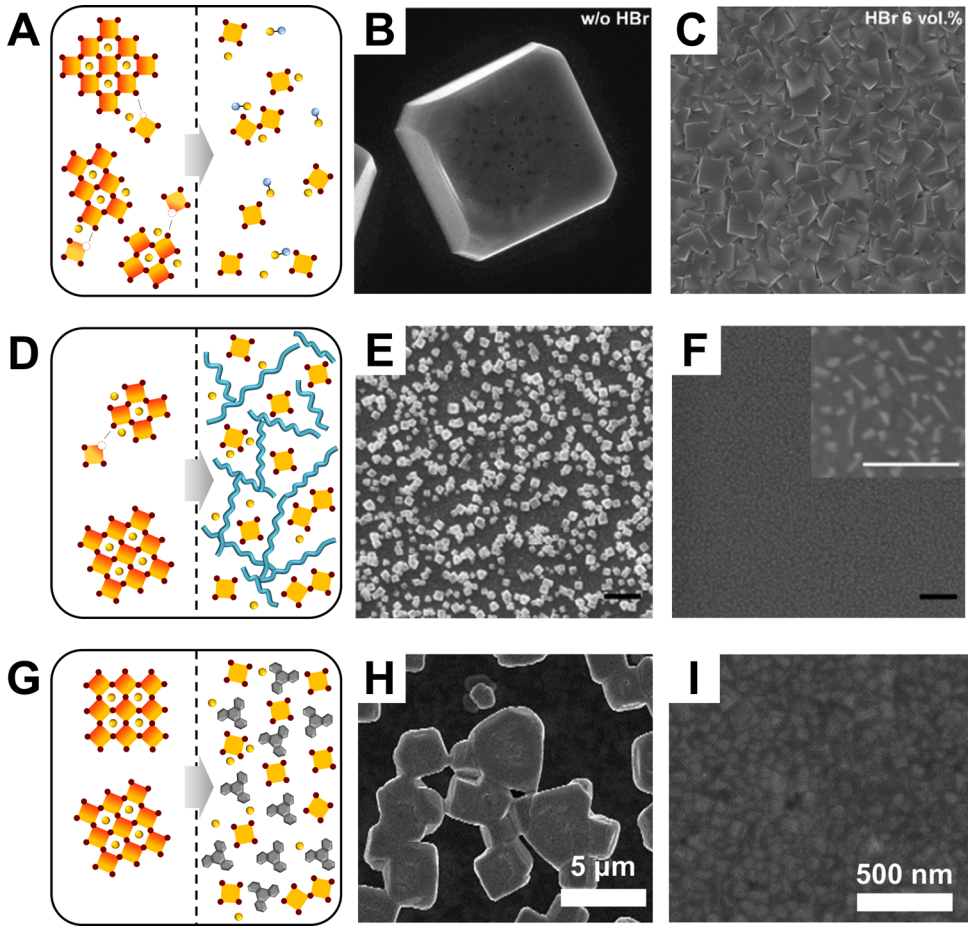


**Figure 3. Schematic illustrations of strategies to control surface morphology using (A) acidic additive such as HBr, (D) polymeric additives such as PIP, and (G) small-molecule additives such as TPBI. Scanning electron microscopy images of $MAPbBr_3$ polycrystalline films with different morpholgical engineering methods. $MAPbBr_3$ films with HBr additive amount of (B) 0 vol % and (C) 6 vol %. (Adapted with permission from ref 87. Copyright 2016 Royal Society of Chemistry.) $MAPbBr_3$ films with PIP additive amount of (E) 0 and (F) 1/2 w/w ratio. (Adapted from ref 92. Copyright 2015 American Chemical Society.) $MAPbBr_3$ polycrystalline films (H) without NCP and (I) with A-NCP. (Adapted with permission from ref 1. Copyright 2015 American Association for the Advancement of Science.)**

15.26 cd/A, whereas PeLEDs without stoichiometry control showed $L_{max}$ = 28.8 cd/m$^2$ and $CE_{max}$ = 0.02 cd/A.[76]

The poor morphology of MHP films can be improved by surface modification of the underlying layers to increase the number of nucleation sites. MHP precursors have a high nucleation barrier and a very poor wettability on underlying hydrophobic surfaces of conventional organic layers, resulting in the discontinuous island growth.[67−69] The difference in interfacial energy causes abrupt partial crystallization with large pinholes during crystal growth, and as a result prohibits full surface coverage of MHP films. UV-ozone treatment to acquire a hydrophilic surface on the underlying layer can improve the wettability of MHP precursors by reducing the interfacial energy and heterogeneous nucleation barrier.[70] This process yields dense nucleation sites and uniform coverage without pinholes. Nickel oxide ($NiO_x$) is a promising hole injection material for PeLEDs to replace the commonly used poly(3,4-ethylenedioxythiophene):poly(styrenesulfonate) (PEDOT:PSS) because the surface energy of $NiO_x$ is much higher than that of PEDOT:PSS and because of other advantages, such as high transmittance >95%, smooth surface morphology, and nonacidic nature. Especially, the nonacidic nature of the underlying $NiO_x$ layer compared with the acidic nature of the underlying PEDOT:PSS layer can result in a lower density of interfacial trap states and related nonradiative recombination at the interface, showing significantly enhanced photostability of MHP films and operational stability of PeLEDs.[77] The hydrophilic $NiO_x$ surface improves the wettability of CsBr and $PbBr_2$ precursors and surface coverage of inorganic $CsPbBr_3$ film, thereby increasing $L_{max}$ to 23 828 cd/m$^2$ and $CE_{max}$ to 9.54 cd/A, whereas PEDOT:PSS-based PeLEDs had $L$ = 14 959 cd/m$^2$ and CE = 2.92 cd/A.[70] A variety of candidates with hydrophilic surfaces, such as poly[(9,9-bis(3′-(*N*,*N*-dimethylamino)propyl)-2,7-fluorene)-*alt*-2,7-(9,9-dioctylfluorene)] (PFN) and $LiCoO_2$, can be substituted for PEDOT:PSS or other hydrophobic HTLs.[78−80]

Also, the crystallization kinetics of MHP films can be precisely controlled by choosing an underlying layer that is soluble in a polar solvent. Poly(styrenesulfonate)-grafted polyaniline (PSS-*g*-PANI) is a self-doped conducting polymer that can be soluble in DMSO, so its film can be partially dissolved by a base solvent of DMSO. As a result, the evaporation rate of the solvent can be retarded. With a delayed evaporation of DMSO during a spin-coating process, high density of nuclei can participate in crystal growth for smaller grains with uniform surface morphology.[81] Therefore, two-times improved device efficiency of 14.3 cd/A was achieved



DOI: 10.1021/acsenergylett.9b00518
*ACS Energy Lett.* 2019, 4, 1134−1149

with PeLEDs based on PSS-*g*-PANI HTL compared to that of pristine PeLEDs based on PEDOT:PSS HTL.[82]

Inserting a hydrophilic insulating polymer layer under the MHP layer is another promising method to modify the surface energy of the underlying layer. Deposition of a hydrophilic polyvinyl pyrrolidine (PVP) interlayer induced a good wetting property with the hydrophilic MHP precursor solution and yielded uniform $CsPbBr_3$ crystal growth with a low density of pinholes; therefore, nonradiative recombination losses were suppressed, and ultrahigh $L_{max}$ = 91 000 cd/m$^2$ and $EQE_{max}$ = 10.4% were achieved.[71]

Addition of stabilizers to the MHP precursor solution to control the crystal growth of MHPs is an effective way to achieve a uniform and smooth surface morphology. When the MHP precursor solution is synthesized with an equimolar ratio of MAI:$PbI_2$, the precursor solution usually forms a mesoscale colloid which then disperses.[83] These mesoscale colloids can participate in nucleation and yield of large crystals that have poor morphology.[84,85] Addition of an excess of MA organic cation to the MHP precursor solutions can decrease the size of the colloids that are dispersed in it, so film morphology can be improved. Acidic additives such as hydroiodic (HI) or hydrobromic (HBr) acid can help to dissolve the colloids, which act as nucleation sites and thus increase the supersaturation concentration of precursor solution during the deposition process and suppress fast crystallization.[84,86] Addition of 6 vol % HBr into the MABr:$PbBr_2$:DMF precursor solution can improve the solubility of the precursors by effectively dissolving the inorganic component, so a dense and uniform $MAPbBr_3$ film with reduced grain size of 500 nm was achieved; the PeLEDs had $L_{max}$ = 3490 cd/m$^2$ and $CE_{max}$ = 0.43 cd/A (Figure 3A−C).[87]

An MHP film with smooth surface morphology can be also deposited by vapor-assisted sequential deposition; this method is useful for mass production with high reproducibility.[88−91] To perform this method, thermally vaporized MAX (X = Cl, Br, I) flows across the surface of a spin-coated $PbX_2$ layer and then diffuses into the underlying $PbX_2$ layer to form a $MAPbX_3$ film by a dissolution−recrystallization mechanism. During this process, if the evaporation time of MABr powder is insufficient (i.e., the concentration of MABr vapor is low), then initially formed $MAPbBr_3$ crystals hinder the diffusion of MABr into the $PbBr_2$ layer and the $MAPbBr_3$ film can retain unreacted $PbBr_2$. The evaporation temperature can be controlled in the range of 120−180 °C to further modify the surface morphology to achieve a smooth and pinhole-free $MAPbBr_3$ film. Therefore, growth parameters such as the evaporation time of MABr vapor and optimized reaction temperature should be precisely optimized to fully convert the $PbBr_2$ layer to a high-quality $MAPbBr_3$ film.

Another strategy to improve the surface morphology by control of crystallization kinetics is to retard crystal growth rate to avoid abrupt crystal growth, which results in a rough surface morphology. Polymeric additives are effective to retard crystal growth of MHPs for the formation of pinhole-free thin films. When a polymeric additive such as poly(ethylene glycol) (PEG), PVK, polyimide precursor (PIP), PVP, or poly(2-hydroxyethyl methacrylate) (poly-HEMA) is added to the MHP precursor solution, its viscosity increases and the interaction between perovskite precursors is hindered, so crystal growth rate can be significantly reduced.[4,92−95] Moreover, polymeric additives significantly interrupt diffusion of MHP precursors during spin-coating and thermal treatment processes. As a result, formation of pinholes can be effectively suppressed, and current leakage can be reduced in PeLEDs. The addition of PIP effectively reduced the crystal size from 250 nm in the large cuboids of pure MHP thin film to 60 nm in PIP:MHP film with weight ratio of 1:2 (Figure 3D−F).[92] This process doubled the EQE of 1% in the $MAPbBr_3$:PIP PeLED, compared to pure $MAPbBr_3$ PeLEDs.[92] Also, incorporation of 0.5−3 wt % PEO into MHPs reduced the crystal size from 2 $\mu$m to 100 nm and yielded uniformly dispersed nanosized grains with film coverage >95%.[96,97] By the mixing of a PEO:DMSO additive solution with a $CsPbBr_3$:DMSO precursor solution before spin-coating, uniform and pinhole-free $CsPbBr_3$ films with high PLQY of 60% were formed by a one-step spin-coating process.[98] This method yielded a fully covered and smooth $CsPbBr_3$−PEO film, suppressed the interfacial quenching and leakage current, and achieved $L_{max}$ = 53525 cd/m$^2$ and $EQE_{max}$ = 4.26%.

The crystallization process can also be retarded using Lewis base additives such as dimethyl siloxane (DMSO), thiourea, and pyridine, which react with lead halide precursors to form a Lewis acid−base adduct.[99−101] The lone-pair electrons in the Lewis base additive are shared with Pb atoms of lead halide precursors by dative bonding, so Lewis acid−base adducts form. The strength of the dative bonds depends on the Lewis basicity, so adduct formation energy can increase as the basicity of the Lewis base additive increases. The Lewis acid−base adduct approach has been mainly reported for the development of solar cell applications, but their retarded crystallization process could be also applicable to PeLEDs by enabling easy control of grain size and passivating defects to reduce low nonradiative recombination losses.[102]

After the formation of MHP films, the film morphology can be also improved with post vapor treatment to remove pinholes and induce further chemical reaction. Residual base solvent of DMSO can make pinholes after the crystallization because of its high boiling point and formation of intermediate phase with $MAPbX_3$ precursors.[103] The vapor-assisted postannealing method can be an effective way to remove pinholes and achieve a closely packed surface morphology by simultaneously rinsing residual DMSO with vaporized other nonpolar solvents such as chlorobenzene (CB).[103] Moreover, providing MA vapor onto $MAPbBr_3$ films can effectively heal and reconstruct the defective grain boundaries, including voids or pinholes arising from insufficient chemical reaction or residual DMSO.[104]

To further develop the crystallization−retardation method, semiconducting small-molecule additives such as TPBI or bathocuproine (BCP) with antisolvent-induced crystallization (i.e., solvent engineering) can be used.[30,105] The crystallization kinetics can be simultaneously controlled by both the small molecules acting as inhibitor and the antisolvent changing the solubility of perovskite precursors, helping make MHP thin films with pinhole-free, closely packed, and uniform surface coverage by controlling the crystallization and washing the base solvent during the spin-coating process.[72−74] Nanocrystal pinning (NCP) is an effective method to control the crystallization kinetics, and thereby it can form the pinhole-free surface morphology of the $MAPbBr_3$ film.[1,30] The NCP process can rapidly induce an excess supersaturation state with a high density of nucleation sites, so crystals grow rapidly with smooth surface morphology and complete coverage (Figure 3G,H).[1,30,75] Therefore, when the crystal growth rate is retarded, the nucleation and crystal growth rate can be



DOI: 10.1021/acsenergylett.9b00518
ACS Energy Lett. 2019, 4, 1134−1149

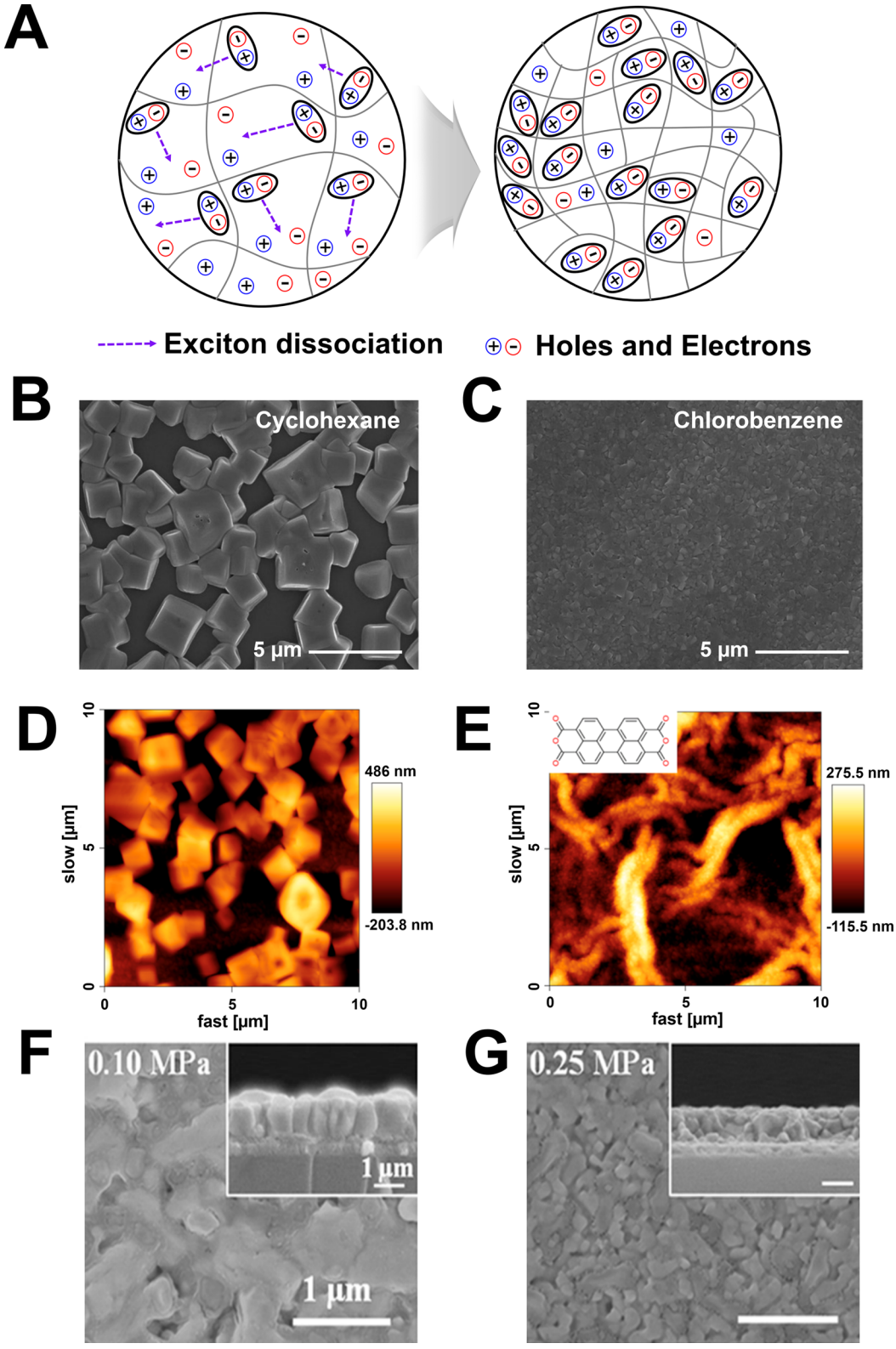


**Figure 4. (A) Schematic illustrations of the spatial exciton confinement in nanograins. Scanning electron microscopy images of $MAPbBr_3$ with different NCP solvents. NCP solvent is (B) cyclohexane or (C) CB. (Adapted with permission from ref 108. Copyright 2017 Royal Society of Chemistry.) Atomic force microscopy images of $MAPbBr_3$ of (D) without A-NCP and (E) with A-NCP. (Adapted from ref 110. Copyright 2017 American Chemical Society.) $MAPbBr_3$−polymer film with different gas pressures. The gas pressure is (F) 0.1 MPa or (G) 0.25 MPa. (Adapted from ref 111. Copyright 2017 American Chemical Society.).**

appropriately controlled by applying the NCP process with optimized dripping time, speed, solvent type, and amount of solvent. With that, incorporation of small-molecule additives dissolved in an antisolvent into the MHP precursor solution can retard the crystal growth by acting as inhibitors. Moreover, the NCP process concurrently modifies surface morphology



DOI: 10.1021/acsenergylett.9b00518
ACS Energy Lett. 2019, 4, 1134−1149

and reduces grain size; those effects will be discussed in the next section.

*Nanograin Engineering.* Small grains effectively confine excitons within grains of 3D MHPs and achieve a high radiative recombination rate to overcome the intrinsic small exciton binding energy and long electron−hole diffusion length (Figure 4A). To reduce grain size and achieve high-efficiency 3D polycrystalline PeLEDs, several methods of solvent engineering, additive engineering, and thermodynamic modification have been developed.[87,106,107]

> Small grains effectively confine excitons within grains of 3D MHPs and achieve a high radiative recombination rate to overcome the intrinsic small exciton binding energy and long electron−hole diffusion length.

During an antisolvent dropping method (i.e., solvent engineering) for nanograin engineering, the crystallization behavior that affects the surface morphology is dependent on the properties of the antisolvent, such as volatility or polarity; that is, a nonpolar solvent can be an effective antisolvent when DMSO or DMF is used as base solvent to dissolve MHP precursors. Cyclohexane, toluene, benzene, CB, and CF can be used as antisolvents when DMSO or DMF are used as a base solvent of MHPs.[108] The relative polarities of antisolvents and base solvents are 0.006 in cyclohexane, 0.099 in toluene, 0.111 in benzene, 0.188 in CB, 0.259 in CF, 0.444 in DMSO, and 0.386 in DMF.[109] When the polarity is too much lower in the antisolvent than in the base solvents of DMSO and DMF that are generally used to dissolve MHP precursors, the antisolvent is relatively immiscible with base solvents and therefore cannot wash them out. Therefore, cyclohexane dripping did not improve the surface morphology compared to the other antisolvents because of its very low polarity, whereas other antisolvents yielded a fully covered and smooth surface morphology with small grains (Figure 4B,C).[108]

The NCP process is an effective solvent engineering method.[1,30] During the NCP process, volatile and nonpolar chloroform (CF) induces rapid crystallization by drastically washing out the polar base solvents (e.g., DMF or DMSO) and thereby significantly influences crystallization kinetics; the embryos can change rapidly to the supersaturated state, so nucleation and crystal growth can easily occur at the interface between the underlying layer and quasi-MHP film during the spin-coating process. Then the surface morphology of $MAPbBr_3$ is improved from randomly distributed micrometer-sized cuboids to well-packed small grains (100−250 nm) with complete coverage.

To further decrease the grain size, TPBI dissolved in CF can be used as an additive; this process is called additive-based NCP (A-NCP). The TPBI additive in the A-NCP process can locate between growing grains, where it impedes crystal coarsening; as a result, the grain size has been decreased to 99 nm and perfect film morphology can be achieved (Figure 3I).[30] The excitons are effectively confined inside small grains by spatial confinement effect, so the electron−hole diffusion length in 3D MHPs can be reduced. Therefore, $MAPbBr_3$ PeLEDs achieved using A-NCP showed high $CE_{max}$ = 42.9 cd/A and $EQE_{max}$ = 8.53%.[1] The TPBI additive is located in the grain boundary region but does not affect perovskite crystal structure; the grain size can be decreased to 86.7 nm with optimized TPBI additive concentration of 0.1 wt % to yield $EQE_{max}$ of 8.79%.[30]

Other additives can be also used in the A-NCP process to control grain size. With perylene-3,4,9,10-tetracarboxylic dianhydride (PTCDA) as an additive for a dripping process, the additive-assisted crystal pinning process greatly reduced grain size to 100−400 nm, compared to 5−10 $\mu$m in pristine $MAPbBr_3$ film without antisolvent treatment (Figure 4D,E).[110] The PTCDA molecular additive can attach to the grain surface by chemical bonding, which can suppress crystal growth. A local emission map of confocal fluorescence microscopy showed homogeneously enhanced PL intensities on the surface of the $MAPbBr_3$ film that had been treated with PTCDA:CF. To give more detailed information about reported NCP methods, the reported additives, solvents, and achieved device efficiencies are summarized in Table 1.

**Table 1. Nanocrystal Pinning (NCP) Methods and Detailed Information**

| NCP methods | precursor solution | solvent | additive | reported device efficiencies |
|---|---|---|---|---|
| solvent-based NCP (S-NCP) | $MAPbBr_3$ | CF | −[a] | 21.4 cd/A,[1] 2.56%[30] |
| S-NCP | $MAPbBr_3$ | CF | −[a] | 15.9 cd/A[104] |
| additive-based NCP (A-NCP) | $MAPbBr_3$ | CF | TPBI | 12.9 cd/A, 8.53%,[1] 8.79%[30] |
| A-NCP | $FA_{0.9}Cs_{0.1}PbBr_3$ | CF | TPBI | 14.5 cd/A, 3.1%[124] |
| A-NCP | $MAPbBr_3$ | CF | PTCDA | 0.02%[110] |
| fast A-NCP | $MAPbBr_3$:TPBI | CF | TPBI | 45.95 cd/A, 11.7%, 87.35 cd/A,[b] 21.81%[b,131] |

[a]The S-NCP method was used without additive. [b]Efficiencies with half-sphere lens.

As an additional effect of solvent engineering, Cl atoms of CB can passivate the defects of the MHP film.[108] This defect passivation effect can be more effective than the use of pure solvent dripping in 3D MHPs because the density of the defective grain boundary region inevitably increases as grain size decreases. Therefore, solvent treatment that results in formation of small grains with smooth film surface concurrently with defect passivation by the antisolvent such as CB may be a promising strategy to fabricate highly efficient 3D polycrystalline PeLEDs.

Gas-assisted crystallization induces fast solvent washing to achieve a high supersaturation state and formation of a large number of nuclei. This method can be used to promote a high nucleation rate with fast crystallization of the MHP film.[91,111] The gas-assisted crystallization method is favorable for mass production and is less toxic than the antisolvent method; therefore, it is more environmentally benign.[1,30,108] In this method, compressed $N_2$ gas is blown over the film surface during the spin-coating process; the purpose is to rapidly remove the base solvent and promote the supersaturation state of the precursor solution.[91,111] When the $N_2$ gas pressure was increased, the average grain size and the thickness of the $MAPbBr_3$−polymer composite film were gradually decreased from 409.8 and 669.8 nm at 0.1 MPa to 79.3 and 509.4 nm at 0.25 MPa (Figure 4F,G).[111] However, after the gas pressure reached 0.3 MPa, the grain size and thickness increased, and


DOI: 10.1021/acsenergylett.9b00518
ACS Energy Lett. 2019, 4, 1134−1149

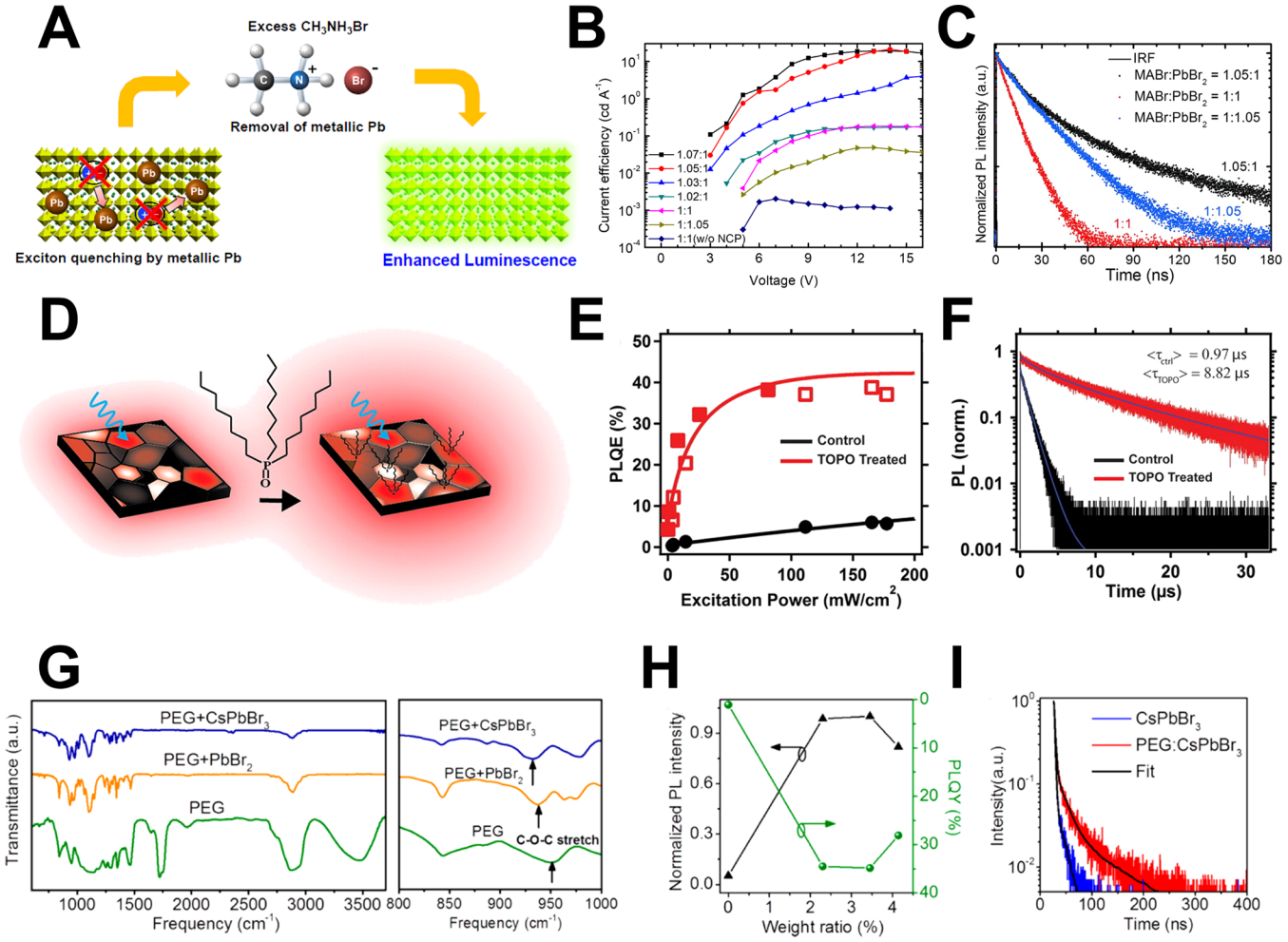


**Figure 5. (A) Schematic illustrations of stoichiometry control using excess MABr to prevent exciton quenching from metallic Pb atoms. (B and C) CE of PeLEDs and PL lifetime of perovskite thin films based on S-NCP and $MAPbBr_3$ nanograin emission layers with varying molar ratio of MABr:$PbBr_2$. (Adapted with permission from ref 1. Copyright 2015 American Association for the Advancement of Science.) (D) Schematic illustration of postligand treatment using tri-n-octylphosphine oxide (TOPO). (E and F) Photoluminescence quantum yield (PLQY) and PL lifetime of control (black) and TOPO-treated films (red). (Adapted from ref 130. Copyright 2016 American Chemical Society.) (G) FTIR spectra of PEG, PEG:$PbBr_2$, and PEG:$CsPbBr_3$ powders. (H) Normalized PL intensity and PLQY as a function of the PEG:$CsPbBr_3$ weight ratio. (I) PL lifetime of neat $CsPbBr_3$ and PEG:$CsPbBr_3$ (0.034:1) films. (Adapted from ref 93. Copyright 2017 American Chemical Society.).**

the surface roughness increased because secondary nucleation may occur onto the precrystallized MHP layer. Therefore, $N_2$ gas pressure must be optimized to deposit efficient MHP films with small grains and smooth surface morphology for high-efficiency PeLEDs. An optimized gas-assisted crystallization process achieved $CE_{max}$ = 1.12 cd/A and $L_{max}$ = 6800 cd/m$^2$ for PeLED with a $MAPbBr_3$−polymer composite film (vs CE = 0.38 cd/A without gas-assisted crystallization).

The properties of MHP films can be significantly influenced by film deposition methods. A two-step deposition method that deposits AX (A = MA, FA, Cs; X = Cl, Br, I) precursor solutions onto a predeposited $PbX_2$ layer is an effective method to control the grain size and surface morphology. Factors such as reaction temperature and loading time before spinning during spin-casting affect the reaction mechanism between two precursor layers.[112,113] The two-step deposition method has high reproducibility due to the precise controllability of crystallization kinetics.[114,115] In particular, the underlying $PbX_2$ surface can provide dense and uniform nucleation sites, so the homogeneous nucleation and crystal growth can be accelerated. When MABr:isopropyl alcohol precursor solution was spin-coated onto the predeposited $PbBr_2$ layer to deposit a $MAPbBr_3$ film, the grain size of the $MAPbBr_3$ film was dramatically decreased to 187 nm, whereas the one-step processed $MAPbBr_3$ film showed the larger grain size of 660 nm.[116]

Another way to control crystallization kinetics is a modulation of precursor sources. The precursors of CsBr and $PbBr_2$ have been generally used to make a $CsPbBr_3$ film. As a source of $CsPbBr_3$ precursors, cesium trifluoroacetate (CsTFA) can be used instead of the CsBr precursor.[117] A CsTFA-based $CsPbBr_3$ film can be effectively formed without forming the intermediate phase (i.e., CsBr·$PbBr_2$·DMSO complex) because of a strong interaction between $TFA^-$ ($CF_3COO^-$) and $Pb^{2+}$. Therefore, the direct conversion into $CsPbBr_3$ at room temperature can accelerate crystallization resulting in high nucleation density, so the CsTFA-based $CsPbBr_3$ films have smooth and smaller grain size (∼60 nm). As a result, the CsTFA-based $CsPbBr_3$ PeLEDs achieved $CE_{max}$ = 32.0 cd/A and $EQE_{max}$ = 10.5%.



DOI: 10.1021/acsenergylett.9b00518
ACS Energy Lett. 2019, 4, 1134−1149

We expect that nanograin engineering by kinetically controlling the crystallization mechanism, combined with deposition process, will be a very important approach to realize highly efficient 3D polycrystalline PeLEDs.

*Chemical Modification*. One challenging aspect of polycrystalline MHP thin films is that they inevitably form high-density defect states. Furthermore, MHP crystals have a polar and soft ionic lattice with lattice tilting and distortion which can result in atomic vacancies and high chemical reactivity, so they are vulnerable.[118] Therefore, the perovskite structure has various ionic trap states as well as the defect states.[119] Charge carriers can be easily trapped or quenched by trap states such as metallic interstitial defects or halide vacancies; as a result, EL efficiency can decrease drastically.[120]

One efficient strategy to increase EL efficiency is to remove metallic quenching sites such as metallic Pb atoms in the perovskite structure. Metallic atoms that remain after incomplete reaction between precursors can act as a strong quencher for excitons by dipole−dipole interaction, which facilitates nonradiative recombination loss.[1,121] Stoichiometry engineering using excess organic cations has been used to remove metallic Pb atoms and reduce exciton quenching (Figure 5A).[1,101,122] PL lifetimes extracted from transient PL data have shown that uncoordinated metallic Pb atoms cause strong nonradiative recombination. PL lifetime can be increased by removing the metallic Pb atoms; the increase in device efficiency can be ascribed to reduction in exciton quenching by the fine stoichiometry control (Figure 5B,C).

Compositional engineering using a different composite system for a stable crystal structure can also enhance the intrinsic chemical stability and suppress the electronic trap states in a perovskite lattice. Substitution of widely used MA cation with other cations, including $FA^+$, $Cs^+$, rubidium ($Rb^+$), potassium ($K^+$) or a mixture of them, has shown to be effective for the enhanced structural stability and photophysical properties.[53,123] In particular, systematic analysis on structural and optical properties of $FA_xCs_{1-x}PbBr_3$ or $FA_xRb_{1-x}PbBr_3$ revealed that incorporating a small amount of alkali cations into perovskite crystals can effectively stabilize the chemical state of $Pb^{2+}$ ions and $PbBr_6$ octahedra, resulting in the low trap density and enhanced EL efficiency with suppressed photoinduced and electrically driven degradation.[32,124] Moreover, central Pb substitution with other divalent metals such as cadmium (Cd) or zinc (Zn) reported in solar cell applications has indicated the possibility of further structural stabilization and enhancement of photophysical properties of 3D MHPs.[125]

Chemically passivating defect states at the grain boundaries is also important because nanograin engineering inevitably causes a high density of grain boundary regions.[126]

Chemically passivating defect states at the grain boundaries is also important because nanograin engineering inevitably causes a high density of grain boundary regions.

Uncoordinated ions occur at the grain surface, mostly as a result of formation of ionic defects with low formation energy such as halogen or MA vacancies and interstitials.[127] These defects can remain charged defects, trap charge carriers, or dissociate excitons into the free charges.[128]

Theoretical studies and direct observation of confocal PL microscopy on the defect chemistry have shown that chemical treatment of nonstoichiometric grain surfaces with uncoordinated Pb atoms can strongly affect the PL efficiency of MHP films.[129] Electron-rich molecules can passivate undercoordinated $Pb^{2+}$ ions in MHPs and thereby suppress charge trapping and nonradiative recombination. Moreover, surface treatment of MHP films with electron-rich Lewis base molecules such as pyridine, thiophene, and tri-n-octylphosphine oxide (TOPO) have dramatically increased the PL lifetimes and PLQYs by neutralizing and deactivating positively charged defects (Figure 5D−F).[102,130] Lewis-basic PEG-doped $CsPbBr_3$ for PeLEDs has been achieved by inducing a dative bonding between electron-rich oxygen atoms and uncoordinated $Pb^{2+}$ defects.[93] Maximum PLQY was much higher (35%) in PEG-doped $CsPbBr_3$ film than in pristine $CsPbBr_3$ film, and the optimized PeLEDs achieved $CE_{max}$ = 19 cd/A and $EQE_{max}$ = 5.34% (Figure 5G−I).[93] In-depth study and experimental investigation of nonradiative losses at the chemical defect states of MHPs are ongoing; the results may further accelerate the development of high-efficiency PeLEDs to achieve high internal quantum efficiency without nonradiative losses.

*Summary and Future Outlook*. 3D polycrystalline MHPs have easier synthesis methods, better coating processabilities, and higher charge transport properties in comparison to low-dimensional MHPs. However, 3D polycrystalline MHPs have intrinsically small exciton binding energy at room temperature, long electron−hole diffusion length, and high refractive index *n* and suffer from defect formation during deposition processes; these shortcomings have limited the EL efficiency of polycrystalline PeLEDs. To overcome those limitations, promising strategies such as optical engineering, charge balance control, morphological and nanograin engineering, and chemical modification have been developed. As a result, during the short and active development period after 2014 for 3D polycrystalline PeLEDs that operate at room temperature, EQEs of 3D polycrystalline PeLEDs have been rapidly improved to >20%, assuming a Lambertian distribution. Moreover, researchers have theoretically and experimentally proven the possibilities of achieving high EQEs of 25% and internal PLQY of 91.9% in polycrystalline PeLEDs.[37] Although those prominent results of 3D polycrystalline PeLEDs have been reported, scientific and technological challenges remain.

The research area of PeLEDs has been divided into three different major subfields: (1) 3D polycrystalline perovskites, (2) quasi-2D perovskites (Ruddlesden−Popper), and (3) 0D perovskites (QDs), and each subfield has its own progress (Figure 1A). The low-dimensional quasi-2D and 0D perovskites in principle do not have the intrinsic limitations in efficiency related to small exciton binding energy and long exciton diffusion length, which can be ideal for high-efficiency emitters. However, the 3D MHPs have those intrinsic limitations in EL efficiency despite their strong advantages of easy synthesis and favorable optical and electrical properties for optoelectronics, as discussed in the above sections. Therefore, the efficient strategies to overcome those fundamental issues in 3D MHP emitters should be further developed to improve the device efficiency of 3D polycrystalline PeLEDs. To improve the EL efficiency of 3D polycrystalline PeLEDs by improving radiative recombination rate, grain size must be decreased to the exciton Bohr diameter (e.g., ∼10 nm for $MAPbBr_3$) to achieve effective spatial confinement of excitons in nanograins. Furthermore, the formation of perfect single-crystalline



DOI: 10.1021/acsenergylett.9b00518
*ACS Energy Lett.* 2019, 4, 1134−1149

nanograins without bulk defects and surface defect passivation by semiconducting additives can be a promising strategy. One way to achieve this goal may be to mimic the core−shell system of low-dimensional MHPs, which are surrounded by bulky organic cations or insulating ligands (i.e., 3D MHP polycrystals surrounded by semiconducting organic additives),[1,30,131] to overcome simultaneously the limited charge transport in low-dimensional PeLEDs and the defective grain boundary passivating in 3D polycrystalline MHP films. Small nanograins surrounded by organic semiconducting additives will also decrease *n* of the 3D MHP films; we expect that the organic semiconducting additives can reduce the density of the MHP films because low-*n* organic additives at the grain boundary region can effectively separate the high-*n* MHP nanograins, thereby reducing *n*. A low *n* can reduce the waveguide mode optical loss at the interface between MHP EMLs and adjacent organic layers; the light outcoupling efficiency can then be maximized by simultaneously controlling the thickness of MHP EMLs.

Methods to overcome the morphological limitations can include additive or solvent engineering to stabilize the MHP precursor and precisely control the crystallization kinetics by surface modification of the underlying layer to attain uniform and dense crystallization of MHPs. To inhibit nonradiative recombination at trap sites in MHP films, various strategies can be applied: the fine stoichiometric approach (excess MABr to remove metallic Pb), the chemical passivation of surface defects with additives that have strong Lewis basicity or acidity, and post-treatment of surface defect states with $CH_3NH_2$ vapor or Lewis-base molecules. Thus, achieving defect-free and highly luminescent MHP crystals is one of the highest priorities for highly efficient 3D polycrystalline PeLEDs that do not suffer from nonradiative losses at trap sites.

The strategies to improve EL efficiency in PeLEDs can be effectively accompanied by an improved device lifetime. Possible influences on device lifetime include the following: (1) Effective charge balance, which can induce the uniform recombination throughout the MHP EMLs, can avoid a local charge accumulation that can cause a local electric field accelerating ion migration. (2) A pinhole-free and smooth surface morphology can reduce the local leakage current that causes Joule heating and degrades the thermal stability. (3) Defect passivation can effectively impede an ion migration at the grain boundary region and improve chemical stability; chemically stable MHP films can improve operational device lifetime. In particular, when small nanograins used to achieve high-efficiency 3D polycrystalline PeLEDs are inevitably accompanied by high-density grain boundary region, passivating the grain boundary region can be a promising strategy to simultaneously improve device lifetime by suppressing the migration of ion species.

Although problems with polycrystalline PeLEDs remain to be solved, we expect that multidisciplinary approaches, especially control of light outcoupling, will yield 3D polycrystalline PeLEDs that have an EQE that is comparable to those of OLEDs (>25−30%) and may reach EL efficiencies that are comparable to those of conventional OLEDs. The prospective strategies for 3D polycrystalline PeLEDs may also be effective in other optoelectronic applications of MHPs.

One way to achieve this goal may be to mimic the core−shell system of low-dimensional MHPs, which are surrounded by bulky organic cations or insulating ligands.

## AUTHOR INFORMATION

### Corresponding Author

*E-mail: twlees@snu.ac.kr, taewlees@gmail.com.

### ORCID

Tae-Woo Lee: 0000-0002-6449-6725

### Author Contributions

#M.-H.P., J.S.K., and J.-M.H. contributed equally to this work.

### Notes

The authors declare no competing financial interest.

### Biographies

**Min-Ho Park** is working as a postdoctoral researcher in Materials Science and Engineering (MSE) at Seoul National University, Republic of Korea. He received his Ph.D. (2017) and M.S. (2013) in MSE from Pohang University of Science and Technology (POSTECH), Korea. His research interests include optoelectronic devices using organic or metal halide perovskite materials.

**Joo Sung Kim** received his B.S. (2016) in MSE from POSTECH. He is currently pursuing his integrated Ph.D. in MSE at Seoul National University, Korea. His research interests include organic−inorganic hybrid optoelectronics, organic light-emitting diodes, and optical spectroscopy.

**Jung-Min Heo** received his B.S. (2016) in Advanced Materials Science and Engineering from Sungkyunkwan University, Korea. He received his M.S. (2019) and is currently pursuing his Ph.D. in MSE at Seoul National University, Korea. His research interests include organic−inorganic hybrid perovskite optoelectronics, photophysics in semiconducting materials, and electronic devices.

**Soyeong Ahn** received her B.S (2013) and M.S. (2015) degrees in Chemical Engineering from Kyung Hee University. She is currently a Ph.D. candidate in MSE at POSTECH, Korea. Her current research focuses on solution-processed electronics based on organic and perovskite materials for optoelectronic devices.

**Su-Hun Jeong** received his B.S. (2012) and Ph.D. (2017) in MSE from POSTECH, Korea. He is currently working in MSE at Seoul National University, Korea as a postdoctoral researcher. His current research work is focused on polymeric electrodes for flexible organic and perovskite optoelectronic devices.

**Tae-Woo Lee** is a professor in the department of Materials Science and Engineering at Seoul National University, Korea. He received his Ph.D in Chemical Engineering from KAIST, Korea in 2002. He joined Bell Laboratories, United States as a postdoctoral researcher (2002) and worked at Samsung Advanced Institute of Technology as a member of the research staff (2003−2008). He was an assistant and associate professor in MSE at POSTECH, Korea (~2016). His research focuses on organic, perovskite, and carbon materials and their applications to flexible electronics, printed electronics, displays, solid-state lighting, solar energy conversion devices, and bioinspired neuromorphic devices.

## ACKNOWLEDGMENTS

This work was supported by the National Research Foundation of Korea (NRF) grant funded by the Korea government (Ministry of Science, ICT & Future Planning) (NRF-2016R1A3B1908431); Creative Materials Discovery



DOI: 10.1021/acsenergylett.9b00518
ACS Energy Lett. 2019, 4, 1134−1149

Program through the National Research Foundation of Korea (NRF) funded by the Ministry of Science and ICT (No. 2018M3D1A1058536).

## REFERENCES


(1) Cho, H.; Jeong, S.-H.; Park, M.-H.; Kim, Y.-H.; Wolf, C.; Lee, C.-L.; Heo, J. H.; Sadhanala, A.; Myoung, N.; Yoo, S.; et al. Overcoming the Electroluminescence Efficiency Limitations of Perovskite Light-Emitting Diodes. *Science* **2015**, *350* (6265), 1222−1225.

(2) Tan, Z.-K.; Moghaddam, R. S.; Lai, M. L.; Docampo, P.; Higler, R.; Deschler, F.; Price, M.; Sadhanala, A.; Pazos, L. M.; Credgington, D.; et al. Bright Light-Emitting Diodes Based on Organometal Halide Perovskite. *Nat. Nanotechnol.* **2014**, *9* (9), 687−692.

(3) Yuan, M.; Quan, L. N.; Comin, R.; Walters, G.; Sabatini, R.; Voznyy, O.; Hoogland, S.; Zhao, Y.; Beauregard, E. M.; Kanjanaboos, P.; et al. Perovskite Energy Funnels for Efficient Light-Emitting Diodes. *Nat. Nanotechnol.* **2016**, *11* (10), 872−877.

(4) Xiao, Z.; Kerner, R. A.; Zhao, L.; Tran, N. L.; Lee, K. M.; Koh, T.-W.; Scholes, G. D.; Rand, B. P. Efficient Perovskite Light-Emitting Diodes Featuring Nanometre-Sized Crystallites. *Nat. Photonics* **2017**, *11* (2), 108−115.

(5) Xing, G.; Wu, B.; Wu, X.; Li, M.; Du, B.; Wei, Q.; Guo, J.; Yeow, E. K. L.; Sum, T. C.; Huang, W. Transcending the Slow Bimolecular Recombination in Lead-Halide Perovskites for Electroluminescence. *Nat. Commun.* **2017**, *8*, 14558.

(6) He, H.; Yu, Q.; Li, H.; Li, J.; Si, J.; Jin, Y.; Wang, N.; Wang, J.; He, J.; Wang, X.; et al. Exciton Localization in Solution-Processed Organolead Trihalide Perovskites. *Nat. Commun.* **2016**, *7* (1), 10896.

(7) D'Innocenzo, V.; Grancini, G.; Alcocer, M. J. P.; Kandada, A. R. S.; Stranks, S. D.; Lee, M. M.; Lanzani, G.; Snaith, H. J.; Petrozza, A. Excitons versus Free Charges in Organo-Lead Tri-Halide Perovskites. *Nat. Commun.* **2014**, *5*, 3586.

(8) Saparov, B.; Mitzi, D. B. Organic−Inorganic Perovskites: Structural Versatility for Functional Materials Design. *Chem. Rev.* **2016**, *116* (7), 4558−4596.

(9) Li, C.; Lu, X.; Ding, W.; Feng, L.; Gao, Y.; Guo, Z. Formability of $ABX_3$ (X = F, Cl, Br, I) Halide Perovskites. *Acta Crystallogr., Sect. B: Struct. Sci.* **2008**, *64* (6), 702−707.

(10) Chen, Q.; De Marco, N.; Yang, Y.; Song, T.-B.; Chen, C. C.; Zhao, H.; Hong, Z.; Zhou, H.; Yang, Y. Under the Spotlight: The Organic-Inorganic Hybrid Halide Perovskite for Optoelectronic Applications. *Nano Today* **2015**, *10* (3), 355−396.

(11) Travis, W.; Glover, E. N. K.; Bronstein, H.; Scanlon, D. O.; Palgrave, R. G. On the Application of the Tolerance Factor to Inorganic and Hybrid Halide Perovskites: A Revised System. *Chem. Sci.* **2016**, *7* (7), 4548−4556.

(12) Becker, M.; Klüner, T.; Wark, M. Formation of Hybrid $ABX_3$ Perovskite Compounds for Solar Cell Application: First-Principles Calculations of Effective Ionic Radii and Determination of Tolerance Factors. *Dalt. Trans.* **2017**, *46* (11), 3500−3509.

(13) Møller, C. K. Crystal Structure and Photoconductivity of Cæsium Plumbohalides. *Nature* **1958**, *182* (4647), 1436−1436.

(14) Weber, D. $CH_3NH_3SnBr_xI_{3-x}$ (x = 0−3), Ein Sn(II)-System Mit Kubischer Perowskitstruktur/$CH_3NH_3SnBr_xI_{3-x}$ (x = 0−3), a Sn(II)-System with Cubic Perovskite Structure. *Z. Naturforsch., B: J. Chem. Sci.* **1978**, *33* (8), 862−865.

(15) Weber, D. $CH_3NH_3PbX_3$, Ein Pb(II)-System Mit Kubischer Perowskitstruktur/$CH_3NH_3PbX_3$, a Pb(II)-System with Cubic Perovskite Structure. *Z. Naturforsch., B: J. Chem. Sci.* **1978**, *33* (12), 1443−1445.

(16) Hirotsu, S. Far-Infrared Reflectivity Spectra of $CsPbCl_3$. *Phys. Lett. A* **1972**, *41* (1), 55−56.

(17) Heidrich, K.; Künzel, H.; Treusch, J. Optical Properties and Electronic Structure of $CsPbCl_3$ and $CsPbBr_3$. *Solid State Commun.* **1978**, *25* (11), 887−889.

(18) Onoda-Yamamuro, N.; Matsuo, T.; Suga, H. Thermal, Electric, and Dielectric Properties of $CH_3NH_3SnBr_3$ at Low Temperatures. *J. Chem. Thermodyn.* **1991**, *23* (10), 987−999.

(19) Onoda-Yamamuro, N.; Matsuo, T.; Suga, H. Dielectric Study of $CH_3NH_3PbX_3$ (X = Cl, Br, I). *J. Phys. Chem. Solids* **1992**, *53* (7), 935−939.

(20) Hirasawa, M.; Ishihara, T.; Goto, T. Exciton Features in 0-, 2-, and 3-Dimensional Networks of $[PbI_6]^{4-}$ Octahedra. *J. Phys. Soc. Jpn.* **1994**, *63* (10), 3870−3879.

(21) Hong, X.; Ishihara, T.; Nurmikko, A. V. Dielectric Confinement Effect on Excitons in $PbI_4$-Based Layered Semiconductors. *Phys. Rev. B: Condens. Matter Mater. Phys.* **1992**, *45* (12), 6961−6964.

(22) Ishihara, T.; Hong, X.; Ding, J.; Nurmikko, A. V. Dielectric Confinement Effect for Exciton and Biexciton States in $PbI_4$-Based Two-Dimensional Semiconductor Structures. *Surf. Sci.* **1992**, *267* (1−3), 323−326.

(23) Hong, X.; Ishihara, T.; Nurmikko, A. V. Photoconductivity and Electroluminescence in Lead Iodide Based Natural Quantum Well Structures. *Solid State Commun.* **1992**, *84* (6), 657−661.

(24) Era, M.; Morimoto, S.; Tsutsui, T.; Saito, S. Organic-inorganic Heterostructure Electroluminescent Device Using a Layered Perovskite Semiconductor $(C_6H_5C_2H_4NH_3)_2PbI_4$. *Appl. Phys. Lett.* **1994**, *65* (6), 676−678.

(25) Hattori, T.; Taira, T.; Era, M.; Tsutsui, T.; Saito, S. Highly Efficient Electroluminescence from a Heterostructure Device Combined with Emissive Layered-Perovskite and an Electron-Transporting Organic Compound. *Chem. Phys. Lett.* **1996**, *254* (1−2), 103−108.

(26) Chondroudis, K.; Mitzi, D. B. Electroluminescence from an Organic−Inorganic Perovskite Incorporating a Quaterthiophene Dye within Lead Halide Perovskite Layers. *Chem. Mater.* **1999**, *11* (11), 3028−3030.

(27) Brenner, T. M.; Egger, D. A.; Kronik, L.; Hodes, G.; Cahen, D. Hybrid Organic—inorganic Perovskites: Low-Cost Semiconductors with Intriguing Charge-Transport Properties. *Nat. Rev. Mater.* **2016**, *1* (1), 15007.

(28) Kim, Y.-H.; Cho, H.; Heo, J. H.; Kim, T.-S.; Myoung, N.; Lee, C.-L.; Im, S. H.; Lee, T.-W. Multicolored Organic/Inorganic Hybrid Perovskite Light-Emitting Diodes. *Adv. Mater.* **2015**, *27* (7), 1248−1254.

(29) Seo, H.-K.; Kim, H.; Lee, J.; Park, M.-H.; Jeong, S.-H.; Kim, Y.-H.; Kwon, S.-J.; Han, T.-H.; Yoo, S.; Lee, T.-W. Efficient Flexible Organic/Inorganic Hybrid Perovskite Light-Emitting Diodes Based on Graphene Anode. *Adv. Mater.* **2017**, *29* (12), 1605587.

(30) Park, M.-H.; Jeong, S.-H.; Seo, H.-K.; Wolf, C.; Kim, Y.-H.; Kim, H.; Byun, J.; Kim, J. S.; Cho, H.; Lee, T.-W. Unravelling Additive-Based Nanocrystal Pinning for High Efficiency Organic-Inorganic Halide Perovskite Light-Emitting Diodes. *Nano Energy* **2017**, *42*, 157−165.

(31) Meng, L.; Yao, E.-P.; Hong, Z.; Chen, H.; Sun, P.; Yang, Z.; Li, G.; Yang, Y. Pure Formamidinium-Based Perovskite Light-Emitting Diodes with High Efficiency and Low Driving Voltage. *Adv. Mater.* **2017**, *29* (4), 1603826.

(32) Shi, Y.; Xi, J.; Lei, T.; Yuan, F.; Dai, J.; Ran, C.; Dong, H.; Jiao, B.; Hou, X.; Wu, Z. Rubidium Doping for Enhanced Performance of Highly Efficient Formamidinium-Based Perovskite Light-Emitting Diodes. *ACS Appl. Mater. Interfaces* **2018**, *10* (11), 9849−9857.

(33) Lin, K.; Xing, J.; Quan, L. N.; de Arquer, F. P. G.; Gong, X.; Lu, J.; Xie, L.; Zhao, W.; Zhang, D.; Yan, C.; et al. Perovskite Light-Emitting Diodes with External Quantum Efficiency Exceeding 20%. *Nature* **2018**, *562* (7726), 245−248.

(34) Cao, Y.; Wang, N.; Tian, H.; Guo, J.; Wei, Y.; Chen, H.; Miao, Y.; Zou, W.; Pan, K.; He, Y.; et al. Perovskite Light-Emitting Diodes Based on Spontaneously Formed Submicrometre-Scale Structures. *Nature* **2018**, *562* (7726), 249−253.

(35) Chen, P.; Meng, Y.; Ahmadi, M.; Peng, Q.; Gao, C.; Xu, L.; Shao, M.; Xiong, Z.; Hu, B. Charge-Transfer versus Energy-Transfer in Quasi-2D Perovskite Light-Emitting Diodes. *Nano Energy* **2018**, *50*, 615−622.




DOI: 10.1021/acsenergylett.9b00518
*ACS Energy Lett.* 2019, 4, 1134−1149

(36) Zhao, X.; Ng, J. D. A.; Friend, R. H.; Tan, Z.-K. Opportunities and Challenges in Perovskite Light-Emitting Devices. *ACS Photonics* **2018**, *5* (10), 3866−3875.
(37) Braly, I. L.; DeQuilettes, D. W.; Pazos-Outón, L. M.; Burke, S.; Ziffer, M. E.; Ginger, D. S.; Hillhouse, H. W. Hybrid Perovskite Films Approaching the Radiative Limit with over 90% Photoluminescence Quantum Efficiency. *Nat. Photonics* **2018**, *12* (6), 355−361.
(38) Zhao, L.; Lee, K. M.; Roh, K.; Khan, S. U. Z.; Rand, B. P. Improved Outcoupling Efficiency and Stability of Perovskite Light-Emitting Diodes Using Thin Emitting Layers. *Adv. Mater.* **2019**, *31*, 1805836.
(39) Shi, X.-B.; Liu, Y.; Yuan, Z.; Liu, X.-K.; Miao, Y.; Wang, J.; Lenk, S.; Reineke, S.; Gao, F. Optical Energy Losses in Organic-Inorganic Hybrid Perovskite Light-Emitting Diodes. *Adv. Opt. Mater.* **2018**, *6* (17), 1800667.
(40) Vincent, A.; Babu, S.; Brinley, E.; Karakoti, A.; Deshpande, S.; Seal, S. Role of Catalyst on Refractive Index Tunability of Porous Silica Antireflective Coatings by Sol−Gel Technique. *J. Phys. Chem. C* **2007**, *111* (23), 8291−8298.
(41) Yu, S.; Wong, T. K. S.; Pita, K.; Hu, X. Synthesis of Organically Modified Mesoporous Silica as a Low Dielectric Constant Intermetal Dielectric. *J. Vac. Sci. Technol., B: Microelectron. Process. Phenom.* **2002**, *20* (5), 2036.
(42) Chiang, K.-M.; Hsu, B.-W.; Chang, Y.-A.; Yang, L.; Tsai, W.-L.; Lin, H.-W. Vacuum-Deposited Organometallic Halide Perovskite Light-Emitting Devices. *ACS Appl. Mater. Interfaces* **2017**, *9* (46), 40516−40522.
(43) Almutlaq, J.; Yin, J.; Mohammed, O. F.; Bakr, O. M. The Benefit and Challenges of Zero-Dimensional Perovskites. *J. Phys. Chem. Lett.* **2018**, *9* (14), 4131−4138.
(44) Kumar, S.; Jagielski, J.; Yakunin, S.; Rice, P.; Chiu, Y.-C.; Wang, M.; Nedelcu, G.; Kim, Y.; Lin, S.; Santos, E. J. G.; et al. Efficient Blue Electroluminescence Using Quantum-Confined Two-Dimensional Perovskites. *ACS Nano* **2016**, *10* (10), 9720−9729.
(45) Sum, T. C.; Mathews, N. Advancements in Perovskite Solar Cells: Photophysics behind the Photovoltaics. *Energy Environ. Sci.* **2014**, *7* (8), 2518−2534.
(46) Byun, J.; Cho, H.; Wolf, C.; Jang, M.; Sadhanala, A.; Friend, R. H.; Yang, H.; Lee, T.-W. Efficient Visible Quasi-2D Perovskite Light-Emitting Diodes. *Adv. Mater.* **2016**, *28* (34), 7515−7520.
(47) Kim, Y.-H.; Wolf, C.; Kim, Y.-T.; Cho, H.; Kwon, W.; Do, S.; Sadhanala, A.; Park, C. G.; Rhee, S.-W.; Im, S. H.; et al. Highly Efficient Light-Emitting Diodes of Colloidal Metal−Halide Perovskite Nanocrystals beyond Quantum Size. *ACS Nano* **2017**, *11* (7), 6586−6593.
(48) Kim, Y.-H.; Lee, G.-H.; Kim, Y.-T.; Wolf, C.; Yun, H. J.; Kwon, W.; Park, C. G.; Lee, T.-W. High Efficiency Perovskite Light-Emitting Diodes of Ligand-Engineered Colloidal Formamidinium Lead Bromide Nanoparticles. *Nano Energy* **2017**, *38*, 51−58.
(49) Shan, Q.; Song, J.; Zou, Y.; Li, J.; Xu, L.; Xue, J.; Dong, Y.; Han, B.; Chen, J.; Zeng, H. High Performance Metal Halide Perovskite Light-Emitting Diode: From Material Design to Device Optimization. *Small* **2017**, *13* (45), 1701770.
(50) Richter, J. M.; Abdi-Jalebi, M.; Sadhanala, A.; Tabachnyk, M.; Rivett, J. P. H.; Pazos-Outón, L. M.; Gödel, K. C.; Price, M.; Deschler, F.; Friend, R. H. Enhancing Photoluminescence Yields in Lead Halide Perovskites by Photon Recycling and Light Out-Coupling. *Nat. Commun.* **2016**, *7* (1), 13941.
(51) Yun, J. S.; Ho-Baillie, A.; Huang, S.; Woo, S. H.; Heo, Y.; Seidel, J.; Huang, F.; Cheng, Y.-B.; Green, M. A. Benefit of Grain Boundaries in Organic−Inorganic Halide Planar Perovskite Solar Cells. *J. Phys. Chem. Lett.* **2015**, *6* (5), 875−880.
(52) Wang, Z.; Wang, F.; Sun, W.; Ni, R.; Hu, S.; Liu, J.; Zhang, B.; Alsaed, A.; Hayat, T.; Tan, Z. Manipulating the Trade-off Between Quantum Yield and Electrical Conductivity for High-Brightness Quasi-2D Perovskite Light-Emitting Diodes. *Adv. Funct. Mater.* **2018**, *28* (47), 1804187.
(53) Abdi-Jalebi, M.; Andaji-Garmaroudi, Z.; Cacovich, S.; Stavrakas, C.; Philippe, B.; Richter, J. M.; Alsari, M.; Booker, E. P.; Hutter, E. M.; Pearson, A. J.; et al. Maximizing and Stabilizing Luminescence from Halide Perovskites with Potassium Passivation. *Nature* **2018**, *555* (7697), 497−501.
(54) Ball, J. M.; Petrozza, A. Defects in Perovskite-Halides and Their Effects in Solar Cells. *Nat. Energy* **2016**, *1* (11), 16149.
(55) Piatkowski, P.; Cohen, B.; Ponseca, C. S.; Salado, M.; Kazim, S.; Ahmad, S.; Sundström, V.; Douhal, A. Unraveling Charge Carriers Generation, Diffusion, and Recombination in Formamidinium Lead Triiodide Perovskite Polycrystalline Thin Film. *J. Phys. Chem. Lett.* **2016**, *7* (1), 204−210.
(56) Nie, W.; Tsai, H.; Asadpour, R.; Blancon, J.-C.; Neukirch, A. J.; Gupta, G.; Crochet, J. J.; Chhowalla, M.; Tretiak, S.; Alam, M. A.; et al. High-Efficiency Solution-Processed Perovskite Solar Cells with Millimeter-Scale Grains. *Science* **2015**, *347* (6221), 522−525.
(57) Shi, D.; Adinolfi, V.; Comin, R.; Yuan, M.; Alarousu, E.; Buin, A.; Chen, Y.; Hoogland, S.; Rothenberger, A.; Katsiev, K.; et al. Low Trap-State Density and Long Carrier Diffusion in Organolead Trihalide Perovskite Single Crystals. *Science* **2015**, *347* (6221), 519−522.
(58) Chen, P.; Xiong, Z.; Wu, X.; Shao, M.; Ma, X.; Xiong, Z.; Gao, C. Highly Efficient Perovskite Light-Emitting Diodes Incorporating Full Film Coverage and Bipolar Charge Injection. *J. Phys. Chem. Lett.* **2017**, *8* (8), 1810−1818.
(59) Salim, T.; Sun, S.; Abe, Y.; Krishna, A.; Grimsdale, A. C.; Lam, Y. M. Perovskite-Based Solar Cells: Impact of Morphology and Device Architecture on Device Performance. *J. Mater. Chem. A* **2015**, *3* (17), 8943−8969.
(60) Eperon, G. E.; Burlakov, V. M.; Docampo, P.; Goriely, A.; Snaith, H. J. Morphological Control for High Performance, Solution-Processed Planar Heterojunction Perovskite Solar Cells. *Adv. Funct. Mater.* **2014**, *24* (1), 151−157.
(61) Lee, T.-W.; Noh, T.; Shin, H.-W.; Kwon, O.; Park, J.-J.; Choi, B.-K.; Kim, M.-S.; Shin, D. W.; Kim, Y.-R. Characteristics of Solution-Processed Small-Molecule Organic Films and Light-Emitting Diodes Compared with Their Vacuum-Deposited Counterparts. *Adv. Funct. Mater.* **2009**, *19* (10), 1625−1630.
(62) Duan, L.; Hou, L.; Lee, T.-W.; Qiao, J.; Zhang, D.; Dong, G.; Wang, L.; Qiu, Y. Solution Processable Small Molecules for Organic Light-Emitting Diodes. *J. Mater. Chem.* **2010**, *20* (31), 6392.
(63) Yu, J. C.; Kim, D. B.; Baek, G.; Lee, B. R.; Jung, E. D.; Lee, S.; Chu, J. H.; Lee, D. K.; Choi, K. J.; Cho, S.; et al. High-Performance Planar Perovskite Optoelectronic Devices: A Morphological and Interfacial Control by Polar Solvent Treatment. *Adv. Mater.* **2015**, *27* (23), 3492−3500.
(64) Jonda, C.; Mayer, A. B. R.; Stolz, U.; Elschner, A.; Karbach, A. Surface Roughness Effects and Their Influence on the Degradation of Organic Light Emitting Devices. *J. Mater. Sci.* **2000**, *35* (22), 5645−5651.
(65) Kumawat, N. K.; Jain, N.; Dey, A.; Narasimhan, K. L.; Kabra, D. Quantitative Correlation of Perovskite Film Morphology to Light Emitting Diodes Efficiency Parameters. *Adv. Funct. Mater.* **2017**, *27* (3), 1603219.
(66) Li, J.; Cai, F.; Yang, L.; Ye, F.; Zhang, J.; Gurney, R. S.; Liu, D.; Wang, T. Sodium Bromide Additive Improved Film Morphology and Performance in Perovskite Light-Emitting Diodes. *Appl. Phys. Lett.* **2017**, *111* (5), No. 053301.
(67) Wu, C.-G.; Chiang, C.-H.; Tseng, Z.-L.; Nazeeruddin, M. K.; Hagfeldt, A.; Grätzel, M. High Efficiency Stable Inverted Perovskite Solar Cells without Current Hysteresis. *Energy Environ. Sci.* **2015**, *8* (9), 2725−2733.
(68) Zabihi, F.; Xie, Y.; Gao, S.; Eslamian, M. Morphology, Conductivity, and Wetting Characteristics of PEDOT:PSS Thin Films Deposited by Spin and Spray Coating. *Appl. Surf. Sci.* **2015**, *338*, 163−177.
(69) Liang, P.-W.; Liao, C.-Y.; Chueh, C.-C.; Zuo, F.; Williams, S. T.; Xin, X.-K.; Lin, J.; Jen, A. K.-Y. Additive Enhanced Crystallization of Solution-Processed Perovskite for Highly Efficient Planar-Heterojunction Solar Cells. *Adv. Mater.* **2014**, *26* (22), 3748−3754.


DOI: 10.1021/acsenergylett.9b00518
*ACS Energy Lett.* 2019, 4, 1134−1149

(70) Wang, Z.; Luo, Z.; Zhao, C.; Guo, Q.; Wang, Y.; Wang, F.; Bian, X.; Alsaedi, A.; Hayat, T.; Tan, Z. Efficient and Stable Pure Green All-Inorganic Perovskite $CsPbBr_3$ Light-Emitting Diodes with a Solution-Processed $NiO_x$ Interlayer. *J. Phys. Chem. C* **2017**, *121* (50), 28132−28138.
(71) Zhang, L.; Yang, X.; Jiang, Q.; Wang, P.; Yin, Z.; Zhang, X.; Tan, H.; Yang, Y. M.; Wei, M.; Sutherland, B. R.; et al. Ultra-Bright and Highly Efficient Inorganic Based Perovskite Light-Emitting Diodes. *Nat. Commun.* **2017**, *8*, 15640.
(72) Ummadisingu, A.; Steier, L.; Seo, J.-Y.; Matsui, T.; Abate, A.; Tress, W.; Grätzel, M. The Effect of Illumination on the Formation of Metal Halide Perovskite Films. *Nature* **2017**, *545* (7653), 208−212.
(73) Zheng, X.; Chen, B.; Wu, C.; Priya, S. Room Temperature Fabrication of $CH_3NH_3$ $PbBr_3$ by Anti-Solvent Assisted Crystallization Approach for Perovskite Solar Cells with Fast Response and Small J−V Hysteresis. *Nano Energy* **2015**, *17*, 269−278.
(74) Paek, S.; Schouwink, P.; Athanasopoulou, E. N.; Cho, K. T.; Grancini, G.; Lee, Y.; Zhang, Y.; Stellacci, F.; Nazeeruddin, M. K.; Gao, P. From Nano- to Micrometer Scale: The Role of Antisolvent Treatment on High Performance Perovskite Solar Cells. *Chem. Mater.* **2017**, *29* (8), 3490−3498.
(75) Xiao, M.; Huang, F.; Huang, W.; Dkhissi, Y.; Zhu, Y.; Etheridge, J.; Gray-Weale, A.; Bach, U.; Cheng, Y.-B.; Spiccia, L. A Fast Deposition-Crystallization Procedure for Highly Efficient Lead Iodide Perovskite Thin-Film Solar Cells. *Angew. Chem., Int. Ed.* **2014**, *53* (37), 9898−9903.
(76) Zhao, X.; Zhang, B.; Zhao, R.; Yao, B.; Liu, X.; Liu, J.; Xie, Z. Simple and Efficient Green-Light-Emitting Diodes Based on Thin Organolead Bromide Perovskite Films via Tuning Precursor Ratios and Postannealing Temperature. *J. Phys. Chem. Lett.* **2016**, *7* (21), 4259−4266.
(77) Lee, S.; Kim, D. B.; Hamilton, I.; Daboczi, M.; Nam, Y. S.; Lee, B. R.; Zhao, B.; Jang, C. H.; Friend, R. H.; Kim, J.-S.; et al. Control of Interface Defects for Efficient and Stable Quasi-2D Perovskite Light-Emitting Diodes Using Nickel Oxide Hole Injection Layer. *Adv. Sci.* **2018**, *5* (11), 1801350.
(78) Lee, J.; Kang, H.; Kim, G.; Back, H.; Kim, J.; Hong, S.; Park, B.; Lee, E.; Lee, K. Achieving Large-Area Planar Perovskite Solar Cells by Introducing an Interfacial Compatibilizer. *Adv. Mater.* **2017**, *29* (22), 1606363.
(79) Chiang, C.-H.; Chen, C.-C.; Nazeeruddin, M. K.; Wu, C.-G. A Newly Developed Lithium Cobalt Oxide Super Hydrophilic Film for Large Area, Thermally Stable and Highly Efficient Inverted Perovskite Solar Cells. *J. Mater. Chem. A* **2018**, *6* (28), 13751−13760.
(80) Zou, Y.; Ban, M.; Yang, Y.; Bai, S.; Wu, C.; Han, Y.; Wu, T.; Tan, Y.; Huang, Q.; Gao, X.; et al. Boosting Perovskite Light-Emitting Diode Performance via Tailoring Interfacial Contact. *ACS Appl. Mater. Interfaces* **2018**, *10* (28), 24320−24326.
(81) Ding, B.; Li, Y.; Huang, S.-Y.; Chu, Q.-Q.; Li, C.-X.; Li, C.-J.; Yang, G.-J. Material Nucleation/Growth Competition Tuning towards Highly Reproducible Planar Perovskite Solar Cells with Efficiency Exceeding 20%. *J. Mater. Chem. A* **2017**, *5* (15), 6840−6848.
(82) Ahn, S.; Park, M.; Jeong, S.; Kim, Y.; Park, J.; Kim, S.; Kim, H.; Cho, H.; Wolf, C.; Pei, M.; et al. Fine Control of Perovskite Crystallization and Reducing Luminescence Quenching Using Self-Doped Polyaniline Hole Injection Layer for Efficient Perovskite Light-Emitting Diodes. *Adv. Funct. Mater.* **2019**, *29* (6), 1807535.
(83) Yan, K.; Long, M.; Zhang, T.; Wei, Z.; Chen, H.; Yang, S.; Xu, J. Hybrid Halide Perovskite Solar Cell Precursors: Colloidal Chemistry and Coordination Engineering behind Device Processing for High Efficiency. *J. Am. Chem. Soc.* **2015**, *137* (13), 4460−4468.
(84) McMeekin, D. P.; Wang, Z.; Rehman, W.; Pulvirenti, F.; Patel, J. B.; Noel, N. K.; Johnston, M. B.; Marder, S. R.; Herz, L. M.; Snaith, H. J. Crystallization Kinetics and Morphology Control of Formamidinium-Cesium Mixed-Cation Lead Mixed-Halide Perovskite via Tunability of the Colloidal Precursor Solution. *Adv. Mater.* **2017**, *29* (29), 1607039.
(85) Jeon, Y.-J.; Lee, S.; Kang, R.; Kim, J.-E.; Yeo, J.-S.; Lee, S.-H.; Kim, S.-S.; Yun, J.-M.; Kim, D.-Y. Planar Heterojunction Perovskite Solar Cells with Superior Reproducibility. *Sci. Rep.* **2015**, *4* (1), 6953.
(86) Noel, N. K.; Congiu, M.; Ramadan, A. J.; Fearn, S.; McMeekin, D. P.; Patel, J. B.; Johnston, M. B.; Wenger, B.; Snaith, H. J. Unveiling the Influence of PH on the Crystallization of Hybrid Perovskites, Delivering Low Voltage Loss Photovoltaics. *Joule* **2017**, *1* (2), 328−343.
(87) Yu, J. C.; Kim, D. B.; Jung, E. D.; Lee, B. R.; Song, M. H. High-Performance Perovskite Light-Emitting Diodes via Morphological Control of Perovskite Films. *Nanoscale* **2016**, *8* (13), 7036−7042.
(88) Ji, H.; Shi, Z.; Sun, X.; Li, Y.; Li, S.; Lei, L.; Wu, D.; Xu, T.; Li, X.; Du, G. Vapor-Assisted Solution Approach for High-Quality Perovskite $CH_3NH_3PbBr_3$ Thin Films for High-Performance Green Light-Emitting Diode Applications. *ACS Appl. Mater. Interfaces* **2017**, *9* (49), 42893−42904.
(89) Leyden, M. R.; Meng, L.; Jiang, Y.; Ono, L. K.; Qiu, L.; Juarez-Perez, E. J.; Qin, C.; Adachi, C.; Qi, Y. Methylammonium Lead Bromide Perovskite Light-Emitting Diodes by Chemical Vapor Deposition. *J. Phys. Chem. Lett.* **2017**, *8* (14), 3193−3198.
(90) Li, X.; Bi, D.; Yi, C.; Decoppet, J.-D.; Luo, J.; Zakeeruddin, S. M.; Hagfeldt, A.; Gratzel, M. A Vacuum Flash-Assisted Solution Process for High-Efficiency Large-Area Perovskite Solar Cells. *Science* **2016**, *353* (6294), 58−62.
(91) Ng, Y. F.; Jamaludin, N. F.; Yantara, N.; Li, M.; Irukuvarjula, V. K. R.; Demir, H. V.; Sum, T. C.; Mhaisalkar, S.; Mathews, N. Rapid Crystallization of All-Inorganic $CsPbBr_3$ Perovskite for High-Brightness Light-Emitting Diodes. *ACS Omega* **2017**, *2* (6), 2757−2764.
(92) Li, G.; Tan, Z.-K.; Di, D.; Lai, M. L.; Jiang, L.; Lim, J. H.-W.; Friend, R. H.; Greenham, N. C. Efficient Light-Emitting Diodes Based on Nanocrystalline Perovskite in a Dielectric Polymer Matrix. *Nano Lett.* **2015**, *15* (4), 2640−2644.
(93) Song, L.; Guo, X.; Hu, Y.; Lv, Y.; Lin, J.; Liu, Z.; Fan, Y.; Liu, X. Efficient Inorganic Perovskite Light-Emitting Diodes with Polyethylene Glycol Passivated Ultrathin $CsPbBr_3$ Films. *J. Phys. Chem. Lett.* **2017**, *8* (17), 4148−4154.
(94) Zuo, L.; Guo, H.; DeQuilettes, D. W.; Jariwala, S.; De Marco, N.; Dong, S.; DeBlock, R.; Ginger, D. S.; Dunn, B.; Wang, M.; et al. Polymer-Modified Halide Perovskite Films for Efficient and Stable Planar Heterojunction Solar Cells. *Sci. Adv.* **2017**, *3* (8), No. e1700106.
(95) Zhao, B.; Bai, S.; Kim, V.; Lamboll, R.; Shivanna, R.; Auras, F.; Richter, J. M.; Yang, L.; Dai, L.; Alsari, M.; et al. High-Efficiency Perovskite−polymer Bulk Heterostructure Light-Emitting Diodes. *Nat. Photonics* **2018**, *12* (12), 783−789.
(96) Jeong, B.; Han, H.; Choi, Y. J.; Cho, S. H.; Kim, E. H.; Lee, S. W.; Kim, J. S.; Park, C.; Kim, D.; Park, C. All-Inorganic $CsPbI_3$ Perovskite Phase-Stabilized by Poly(Ethylene Oxide) for Red-Light-Emitting Diodes. *Adv. Funct. Mater.* **2018**, *28* (16), 1706401.
(97) Li, J.; Bade, S. G. R.; Shan, X.; Yu, Z. Single-Layer Light-Emitting Diodes Using Organometal Halide Perovskite/Poly(Ethylene Oxide) Composite Thin Films. *Adv. Mater.* **2015**, *27* (35), 5196−5202.
(98) Ling, Y.; Tian, Y.; Wang, X.; Wang, J. C.; Knox, J. M.; Perez-Orive, F.; Du, Y.; Tan, L.; Hanson, K.; Ma, B.; et al. Enhanced Optical and Electrical Properties of Polymer-Assisted All-Inorganic Perovskites for Light-Emitting Diodes. *Adv. Mater.* **2016**, *28* (40), 8983−8989.
(99) Ahn, N.; Son, D.-Y.; Jang, I.-H.; Kang, S. M.; Choi, M.; Park, N.-G. Highly Reproducible Perovskite Solar Cells with Average Efficiency of 18.3% and Best Efficiency of 19.7% Fabricated via Lewis Base Adduct of Lead(II) Iodide. *J. Am. Chem. Soc.* **2015**, *137* (27), 8696−8699.
(100) Lee, J. W.; Kim, H. S.; Park, N. G. Lewis Acid-Base Adduct Approach for High Efficiency Perovskite Solar Cells. *Acc. Chem. Res.* **2016**, *49* (2), 311−319.
(101) Lee, J.-W.; Choi, Y. J.; Yang, J.; Ham, S.; Jeon, S. K.; Lee, J. Y.; Song, Y.; Ji, E. K.; Yoon, D.; Seo, S.; et al. In-Situ Formed Type I


DOI: 10.1021/acsenergylett.9b00518
*ACS Energy Lett.* 2019, 4, 1134−1149

Nanocrystalline Perovskite Film for Highly Efficient Light-Emitting Diode. *ACS Nano* **2017**, *11* (3), 3311−3319.
(102) Noel, N. K.; Abate, A.; Stranks, S. D.; Parrott, E. S.; Burlakov, V. M.; Goriely, A.; Snaith, H. J. Enhanced Photoluminescence and Solar Cell Performance via Lewis Base Passivation of Organic−Inorganic Lead Halide Perovskites. *ACS Nano* **2014**, *8* (10), 9815−9821.
(103) Lei, J.; Wang, H.; Gao, F.; Liu, S. Improving the Quality of $CH_3NH_3PbI_3$ Films via Chlorobenzene Vapor Annealing. *Phys. Status Solidi A* **2018**, *215* (17), 1700959.
(104) Chih, Y.-K.; Wang, J.-C.; Yang, R.-T.; Liu, C.-C.; Chang, Y.-C.; Fu, Y.-S.; Lai, W.-C.; Chen, P.; Wen, T.-C.; Huang, Y.-C.; et al. $NiO_x$ Electrode Interlayer and $CH_3NH_2/CH_3NH_3PbBr_3$ Interface Treatment to Markedly Advance Hybrid Perovskite-Based Light-Emitting Diodes. *Adv. Mater.* **2016**, *28* (39), 8687−8694.
(105) Singh, S.; Sharma, B.; Banappanavar, G.; Dey, A.; Chakraborty, S.; Narasimhan, K. L.; Bhargava, P.; Kabra, D. Investigation on Organic Molecule Additive for Moisture Stability and Defect Passivation via Physisorption in $CH_3NH_3PbI_3$ Based Perovskite. *ACS Appl. Energy Mater.* **2018**, *1* (5), 1870−1877.
(106) Jeon, N. J.; Noh, J. H.; Kim, Y. C.; Yang, W. S.; Ryu, S.; Seok, S. Il. Solvent Engineering for High-Performance Inorganic−Organic Hybrid Perovskite Solar Cells. *Nat. Mater.* **2014**, *13* (9), 897−903.
(107) Xia, B.; Wu, Z.; Dong, H.; Xi, J.; Wu, W.; Lei, T.; Xi, K.; Yuan, F.; Jiao, B.; Xiao, L.; et al. Formation of Ultrasmooth Perovskite Films toward Highly Efficient Inverted Planar Heterojunction Solar Cells by Micro-Flowing Anti-Solvent Deposition in Air. *J. Mater. Chem. A* **2016**, *4* (17), 6295−6303.
(108) Yu, J. C.; Kim, D. W.; Kim, D. B.; Jung, E. D.; Lee, K.-S.; Lee, S.; Nuzzo, D. Di; Kim, J.-S.; Song, M. H. Effect of the Solvent Used for Fabrication of Perovskite Films by Solvent Dropping on Performance of Perovskite Light-Emitting Diodes. *Nanoscale* **2017**, *9* (5), 2088−2094.
(109) Reichardt, C.; Welton, T. *Solvents and Solvent Effects in Organic Chemistry*; Wiley-VCH Verlag GmbH & Co. KGaA: Weinheim, Germany, 2010.
(110) Kumar, P.; Zhao, B.; Friend, R. H.; Sadhanala, A.; Narayan, K. S. Kinetic Control of Perovskite Thin-Film Morphology and Application in Printable Light-Emitting Diodes. *ACS Energy Lett.* **2017**, *2* (1), 81−87.
(111) Kim, Y. C.; Porte, Y.; Baek, S.-D.; Cho, S. R.; Myoung, J.-M. High-Performance Green Light-Emitting Diodes Based on $MAPbBr_3$−Polymer Composite Films Prepared by Gas-Assisted Crystallization. *ACS Appl. Mater. Interfaces* **2017**, *9* (50), 44106−44113.
(112) Ahn, N.; Kang, S. M.; Lee, J.-W.; Choi, M.; Park, N.-G. Thermodynamic Regulation of $CH_3NH_3PbI_3$ Crystal Growth and Its Effect on Photovoltaic Performance of Perovskite Solar Cells. *J. Mater. Chem. A* **2015**, *3* (39), 19901−19906.
(113) Kim, S.-Y.; Jo, H. J.; Sung, S.-J.; Kim, D.-H. Perspective: Understanding of Ripening Growth Model for Minimum Residual $PbI_2$ and Its Limitation in the Planar Perovskite Solar Cells. *APL Mater.* **2016**, *4* (10), 100901.
(114) Im, J.-H.; Kim, H.-S.; Park, N.-G. Morphology-Photovoltaic Property Correlation in Perovskite Solar Cells: One-Step versus Two-Step Deposition of $CH_3NH_3PbI_3$. *APL Mater.* **2014**, *2* (8), No. 081510.
(115) Im, J.-H.; Jang, I.-H.; Pellet, N.; Grätzel, M.; Park, N.-G. Growth of $CH_3NH_3PbI_3$ Cuboids with Controlled Size for High-Efficiency Perovskite Solar Cells. *Nat. Nanotechnol.* **2014**, *9* (11), 927−932.
(116) Kim, J. S.; Cho, H.; Wolf, C.; Yun, H. J.; Heo, J.-M.; Lee, T.-W. Increased Luminescent Efficiency of Perovskite Light Emitting Diodes Based on Modified Two-Step Deposition Method Providing Gradient Concentration. *APL Mater.* **2018**, *6* (11), 111101.
(117) Wang, H.; Zhang, X.; Wu, Q.; Cao, F.; Yang, D.; Shang, Y.; Ning, Z.; Zhang, W.; Zheng, W.; Yan, Y.; et al. Trifluoroacetate Induced Small-Grained $CsPbBr_3$ Perovskite Films Result in Efficient and Stable Light-Emitting Devices. *Nat. Commun.* **2019**, *10* (1), 665.
(118) Lai, M.; Obliger, A.; Lu, D.; Kley, C. S.; Bischak, C. G.; Kong, Q.; Lei, T.; Dou, L.; Ginsberg, N. S.; Limmer, D. T.; et al. Intrinsic Anion Diffusivity in Lead Halide Perovskites Is Facilitated by a Soft Lattice. *Proc. Natl. Acad. Sci. U. S. A.* **2018**, *115* (47), 11929−11934.
(119) Shi, T.; Yin, W.-J.; Hong, F.; Zhu, K.; Yan, Y. Unipolar Self-Doping Behavior in Perovskite $CH_3NH_3PbBr_3$. *Appl. Phys. Lett.* **2015**, *106* (10), 103902.
(120) Li, W.; Sun, Y.-Y.; Li, L.; Zhou, Z.; Tang, J.; Prezhdo, O. V. Control of Charge Recombination in Perovskites by Oxidation State of Halide Vacancy. *J. Am. Chem. Soc.* **2018**, *140* (46), 15753−15763.
(121) Markov, D. E.; Blom, P. W. M. Migration-Assisted Energy Transfer at Conjugated Polymer/Metal Interfaces. *Phys. Rev. B: Condens. Matter Mater. Phys.* **2005**, *72* (16), 161401.
(122) Meng, F.; Zhang, C.; Chen, D.; Zhu, W.; Yip, H.-L.; Su, S.-J. Combined Optimization of Emission Layer Morphology and Hole-Transport Layer for Enhanced Performance of Perovskite Light-Emitting Diodes. *J. Mater. Chem. C* **2017**, *5* (25), 6169−6175.
(123) Saliba, M.; Matsui, T.; Seo, J.-Y.; Domanski, K.; Correa-Baena, J.-P.; Nazeeruddin, M. K.; Zakeeruddin, S. M.; Tress, W.; Abate, A.; Hagfeldt, A.; et al. Cesium-Containing Triple Cation Perovskite Solar Cells: Improved Stability, Reproducibility and High Efficiency. *Energy Environ. Sci.* **2016**, *9* (6), 1989−1997.
(124) Cho, H.; Kim, J. S.; Wolf, C.; Kim, Y.-H.; Yun, H. J.; Jeong, S.-H.; Sadhanala, A.; Venugopalan, V.; Choi, J. W.; Lee, C.-L.; et al. High-Efficiency Polycrystalline Perovskite Light-Emitting Diodes Based on Mixed Cations. *ACS Nano* **2018**, *12* (3), 2883−2892.
(125) Saidaminov, M. I.; Kim, J.; Jain, A.; Quintero-Bermudez, R.; Tan, H.; Long, G.; Tan, F.; Johnston, A.; Zhao, Y.; Voznyy, O.; et al. Suppression of Atomic Vacancies via Incorporation of Isovalent Small Ions to Increase the Stability of Halide Perovskite Solar Cells in Ambient Air. *Nat. Energy* **2018**, *3* (8), 648−654.
(126) Seager, C. H. Grain Boundaries in Polycrystalline Silicon. *Annu. Rev. Mater. Sci.* **1985**, *15* (1), 271−302.
(127) Liu, Y.; Palotas, K.; Yuan, X.; Hou, T.; Lin, H.; Li, Y.; Lee, S.-T. Atomistic Origins of Surface Defects in $CH_3NH_3PbBr_3$ Perovskite and Their Electronic Structures. *ACS Nano* **2017**, *11* (2), 2060−2065.
(128) Uratani, H.; Yamashita, K. Charge Carrier Trapping at Surface Defects of Perovskite Solar Cell Absorbers: A First-Principles Study. *J. Phys. Chem. Lett.* **2017**, *8* (4), 742−746.
(129) de Quilettes, D. W.; Vorpahl, S. M.; Stranks, S. D.; Nagaoka, H.; Eperon, G. E.; Ziffer, M. E.; Snaith, H. J.; Ginger, D. S. Impact of Microstructure on Local Carrier Lifetime in Perovskite Solar Cells. *Science* **2015**, *348* (6235), 683−686.
(130) deQuilettes, D. W.; Koch, S.; Burke, S.; Paranji, R. K.; Shropshire, A. J.; Ziffer, M. E.; Ginger, D. S. Photoluminescence Lifetimes Exceeding 8 $\mu$s and Quantum Yields Exceeding 30% in Hybrid Perovskite Thin Films by Ligand Passivation. *ACS Energy Lett.* **2016**, *1* (2), 438−444.
(131) Park, M.-H.; Park, J.; Lee, J.; So, H. S.; Kim, H.; Jeong, S.-H.; Han, T.-H.; Wolf, C.; Lee, H.; Yoo, S.; et al. Efficient Perovskite Light-Emitting Diodes Using Polycrystalline Core−Shell-Mimicked Nanograins. *Adv. Funct. Mater.* **2019**, 1902017.


DOI: 10.1021/acsenergylett.9b00518
*ACS Energy Lett.* 2019, 4, 1134−1149